



UPPSALA  
UNIVERSITET

*Digital Comprehensive Summaries of Uppsala Dissertations  
from the Faculty of Science and Technology 1452*

# Mesoporous magnesium carbonate as a drug delivery vehicle for stabilising amorphous drugs and regulating their release rate

PENG ZHANG



ACTA  
UNIVERSITATIS  
UPSALIENSIS  
UPPSALA  
2016

ISSN 1651-6214  
ISBN 978-91-554-9752-1  
urn:nbn:se:uu:diva-303832

Dissertation presented at Uppsala University to be publicly examined in Ång/2001, Ångströmlaboratoriet, Lägerhyddsvägen 1, Uppsala, Friday, 11 November 2016 at 09:30 for the degree of Doctor of Philosophy. The examination will be conducted in English. Faculty examiner: professor Niklas Hedin (Stockholms Universitet).

### **Abstract**

Zhang, P. 2016. Mesoporous magnesium carbonate as a drug delivery vehicle for stabilising amorphous drugs and regulating their release rate. *Digital Comprehensive Summaries of Uppsala Dissertations from the Faculty of Science and Technology* 1452. 68 pp. Uppsala: Acta Universitatis Upsaliensis. ISBN 978-91-554-9752-1.

In today's drug discovery, the number of candidate drugs based on new molecular entities with poor aqueous solubility is increasing. Since poor aqueous solubility of an active pharmaceutical ingredients (APIs) is associated with low bioavailability and thus limits their therapeutic effect, this is often a great challenge in the development of new drugs when oral administration is the preferred route of administration. A number of different strategies have been developed to circumvent this problem where salt formulations of an API is the most widely employed method. However, new strategies are needed since there is no one solution that solves this issue for all substances. In recent time, the concept of stabilizing poorly soluble APIs in their amorphous form has gained a lot of attention since amorphous compounds exhibit a higher apparent solubility compared to their crystalline counterparts. Amorphous substances are prone to crystallize if left in a non-constricted environment and thus need to be stabilized if the amorphous state is to be conserved until administration. Inorganic mesoporous materials have been proposed as an interesting type of excipients that can conserve the amorphous state of APIs.

In this work, the focus was to investigate the possibilities of using a mesoporous type of magnesium carbonate to stabilize the amorphous state of different APIs. Due to the nanometer sized pores in the material, complete conservation of amorphous APIs was obtained. This resulted in both an increase in *in vitro* release rate and a higher solubility of the substances which may translate to both a faster onset of action and an improved therapeutic effect of the APIs in a clinical situation. The long term stability of formulations was also investigated showing promising results.

The results presented in this work show that mesoporous magnesium carbonate represents an interesting type of excipient for oral formulations of APIs with poor aqueous solubility.

*Keywords:* mesoporous, magnesium carbonate, drug delivery, solubility enhancement, bioavailability, pharmacokinetics, diffusion release, controlled release

*Peng Zhang, Department of Engineering Sciences, Nanotechnology and Functional Materials, Box 534, Uppsala University, SE-75121 Uppsala, Sweden.*

© Peng Zhang 2016

ISSN 1651-6214

ISBN 978-91-554-9752-1

urn:nbn:se:uu:diva-303832 (<http://urn.kb.se/resolve?urn=urn:nbn:se:uu:diva-303832>)

*To my family*



# List of Papers

This thesis is based on the following papers, which are referred to in the text by their Roman numerals.

- I     Stabilisation of amorphous ibuprofen in Upsalite, a mesoporous magnesium carbonate, as an approach to increasing the aqueous solubility of poorly soluble drugs  
P. Zhang, J. Forsgren and M. Strømme, *International Journal of Pharmaceutics*, 2014, 10, 185-191
  
- II    Diffusion-controlled drug release from the mesoporous magnesium carbonate Upsalite<sup>®</sup>  
P. Zhang, T. Zardán Gómez de la Torre, J. Forsgren, C. Bergström and M. Strømme, *Journal of Pharmaceutical Sciences*, 2016, 105, 657-663
  
- III   Nanostructure and pore size control of template-free synthesised mesoporous magnesium carbonate  
O. Cheung, P. Zhang, S. Frykstrand, H. Zheng, T. Yang, M. Sommariva, X. Zou and M. Strømme, *RSC Advances*, 2016, 6, 74241-74249
  
- IV    Supersaturation of poorly soluble drugs induced by mesoporous magnesium carbonate  
P. Zhang, T. Zardán Gómez de la Torre, K. Welch, C. Bergström and M. Strømme, *European Journal of Pharmaceutical Sciences*, 2016, doi:10.1016/j.ejps.2016.08.059
  
- V     Amine modification of mesoporous magnesium carbonate and effects on controlled drug release  
M. Vall, P. Zhang, A. Gao, S. Frykstrand, O. Cheung and M. Strømme, 2016, *submitted*

Reprints were made with permission from the respective publishers.

# The author's contribution to the included papers

- I I took part in planning the study, performed the experimental work and took part in the writing of the manuscript.
- II I was responsible for the planning and execution of the study, as well as writing the manuscript.
- III I participated in planning the study and evaluating the results. I performed the experimental work on MMC synthesis and characterisation. I carried out the drug loading and release analysis and took part in writing the manuscript.
- IV I was responsible for the planning and execution of the work, performing the experimental work, evaluating the results, and writing the manuscript.
- V I participated in the planning of the study, carried out the drug loading, characterisation and release study, and took part in evaluating the results and writing the manuscript.

## Also published

### Journal articles

1. Efficient High Active Mass Paper-Based Energy-Storage Devices containing Free-standing Additive-less Polypyrrole-Nanocellulose Electrodes  
Z. Wang, P. Tammela, P. Zhang, M. Strømme and L. Nyholm, *Journal of Material Chemistry A*, 2014, 2, 7711-7716
2. High Areal and Volumetric Capacity Sustainable All-Polymer Paper-Based Supercapacitors  
Z. Wang, P. Tammela, P. Zhang, M. Strømme and L. Nyholm, *Journal of Material Chemistry A*, 2014, 2, 16761-16769
3. Photocatalysis induces bioactivity of an organic polymer based material  
Y. Cai, M. Strømme, P. Zhang, H. Engqvist and K. Welch, *RSC Advances*, 2014, 4, 57715-57723
4. Freestanding nanocellulose-composite fibre reinforced 3D polypyrrole electrodes for energy storage applications  
Z. Wang, P. Tammela, P. Zhang, M. Strømme and L. Nyholm, *Nanoscale*, 2014, 6, 13068-13075
5. Asymmetric supercapacitors based on carbon nanofibre and polypyrrole/nanocellulose composite electrodes  
P. Tammela, Z. Wang, S. Frykstrand, P. Zhang, I-M. Sintorn, L. Nyholm and M. Strømme, *RSC Advances*, 2015, 5, 16405-16413
6. Surface modified nanocellulose fibers yield conducting polymer-based flexible supercapacitors with enhanced capacitances  
Z. Wang, D. Carlsson, P. Tammela, K. Hua, P. Zhang, L. Nyholm and M. Strømme, *ACS Nano*, 2015, 9, 7563-7571
7. Conducting Polymer Paper-Based Cathodes for High-Areal-Capacity Lithium-Organic Batteries  
Z. Wang, C. Xu, P. Tammela, P. Zhang, K. Edström, T. Gustafsson, M. Strømme and L. Nyholm, *Energy Technology*, 2015, 3, 563-569

8. Cytotoxicity, *in vivo* skin irritation and acute systemic toxicity of the mesoporous magnesium carbonate Upsalite<sup>®</sup>  
S. Frykstrand, J. Forsgren, P. Zhang, M. Strømme and N. Ferraz, *Journal of Biomaterials and Nanobiotechnology*, 2015, 6, 257-266
9. Transition from bioinert to bioactive material by tailoring the biological cell response to carboxylated nanocellulose  
K. Hua, I. Rocha, P. Zhang, S. Gustafsson, Y. Ning, M. Strømme, A. Mihranyan and N. Ferraz, *Biomacromolecules*, 2016, 17, 1224-1233
10. Study of mesoporous magnesium carbonate in contact with whole human blood  
S. Frykstrand, J. Forsgren, O. Cheung, P. Zhang, J. Hong, M. Strømme and N. Ferraz, *RSC Advances*, 2016, 6, 52810-52816
11. Solution-processed poly(3,4-ethylenedioxythiophene) nanocomposite paper electrodes for high-capacitance flexible supercapacitors  
Z. Wang, P. Tammela, J. Huo, P. Zhang, M. Strømme and L. Nyholm, *Journal of Materials Chemistry A*, 2016, 4, 1714-1722

#### Conference contributions

1. P. Zhang, J. Forsgren and M. Strømme. (2014) Upsalite<sup>®</sup> - Nanoporous Magnesium Carbonate - as Phase Stabilizer of Amorphous IBU. *Poster presentation* at Bioceramics 26, Barcelona, Spain
2. P. Zhang, J. Forsgren and M. Strømme. (2014) Investigation using Nanoporous Magnesium Carbonate as Phase Stabilizer of Amorphous IBU to improve the solubility. *Poster presentation* at CRS2014 Annual Meeting, Chicago, US
3. P. Zhang, T. Zardán Gómez de la Torre, J. Forsgren, CAS. Bergström and M. Strømme. (2015) Mesoporous Magnesium Carbonate – A Novel Drug Delivery System. *Poster presentation* at CRS2015 Annual Meeting, Scotland, UK
4. P. Zhang, T. Zardán Gómez de la Torre, CAS. Bergström and M. Strømme. (2016) Diffusion controlled drug release from Mesoporous Magnesium Carbonate. *Poster presentation* at CRS2016 Annual Meeting, Seattle, US



## Patent application

Highly porous magnesium carbonate and method of production thereof.  
O. Cheung, P. Zhang, S. Gustafsson, S. Frykstrand Ångström and M.  
Strømme, Patent Application, *submitted*

# Abbreviations

|           |  |
|-----------|--|
| API       | Active pharmaceutical ingredient                         |
| APTES     | (3-Aminopropyl)triethoxysilane                           |
| AUC       | Area under the concentration-time curve                  |
| BCS       | Biopharmaceutics Classification System                   |
| BET       | Branauer-Emmet-Teller                                    |
| CEL       | Celecoxib  |
| CIN       | Cinnarizine  |
| $C_{MAX}$ | Maximum concentration                                    |
| DDS       | Drug-delivery system                                     |
| DFT       | Density functional theory                                |
| DLS       | Dynamic light scattering                                 |
| DSC       | Differential scanning calorimetry                        |
| GRI       | Griseofulvin   |
| HR-TEM    | High resolution TEM                                      |
| IBU       | Ibuprofen  |
| ICP-OES   | Inductively coupled plasma optical emission spectroscopy |
| IR        | Infrared spectroscopy                                    |
| ITZ       | Itraconazole   |
| IUPAC     | International Union of Pure and Applied Chemistry        |
| MMC       | Mesoporous magnesium carbonate                           |
| c-MMC     | Centrifuged mesoporous magnesium carbonate               |
| m-MMC     | Modified mesoporous magnesium carbonate                  |
| PTES      | N-propyltriethoxysilane                                  |
| SEM       | Scanning electron microscopy                             |
| TEM       | Transmission electron microscopy                         |
| TGA       | Thermogravimetric analysis                               |
| $T_{MAX}$ | Time taken to reach the maximum concentration            |
| USP       | United States Pharmacopeia                               |
| XRD       | Powder X-ray diffraction                                 |

# Contents

|   |    |
|---|----|
| 1. Introduction.....  | 13 |
| 2. Aims of the thesis.....  | 15 |
| 3. Background.....  | 16 |
| 3.1 Drug dissolution and bioavailability .....  | 16 |
| 3.2 Formulation procedures for enhancing the solubility of poorly<br>water-soluble drugs..... | 18 |
| 3.2.1 Chemical methods .....  | 19 |
| 3.2.2 Physical methods .....  | 20 |
| 3.3 Approaches to stabilise an amorphous solid .....  | 27 |
| 3.3.1 Polymers .....  | 28 |
| 3.3.2 Surfactants .....   | 28 |
| 3.3.3 Porous materials/Mesoporous materials .....   | 29 |
| 3.4 Magnesium Carbonate.....  | 31 |
| 3.4.1 Magnesium Carbonate Minerals.....   | 31 |
| 3.4.2 Mesoporous Magnesium Carbonate (MMC).....   | 31 |
| 3.4.3 Functionalisation of MMC .....  | 32 |
| 4. Methodology.....   | 34 |
| 4.1 MMC synthesis .....   | 34 |
| 4.2 MMC modification.....   | 34 |
| 4.3 API loading method .....  | 35 |
| 4.4 Materials characterisation.....   | 36 |
| 4.4.1 Powder X-ray diffraction (XRD).....   | 36 |
| 4.4.2 Scanning electron microscopy (SEM).....   | 36 |
| 4.4.3 Nitrogen adsorption/desorption isotherms.....   | 36 |
| 4.4.4 Thermogravimetric analysis (TGA).....   | 37 |
| 4.4.5 Differential scanning calorimetry (DSC).....  | 37 |
| 4.4.6 Dynamic light scattering (DLS).....   | 37 |
| 4.4.7 Infrared spectroscopy (IR).....   | 38 |
| 4.5 Drug-release analysis .....   | 38 |

|   |    |
|---|----|
| 5. Results and Discussion .....   | 39 |
| 5.1 Synthesis, structure and pore-size control of MMC .....             | 39 |
| 5.1.1 Structural characterisation of MMC .....                          | 39 |
| 5.1.2 Pore-size control in MMC .....                                    | 42 |
| 5.1.3 Surface Modification of MMC .....                                 | 44 |
| 5.2 Physical properties of loaded APIs .....                            | 45 |
| 5.2.1 State of loaded APIs .....  | 45 |
| 5.2.2 Characterisation of the porous structure after API loaded .....   | 46 |
| 5.3 <i>In vitro</i> release study .....                                 | 47 |
| 5.3.1 Release mechanism study .....                                     | 47 |
| 5.3.2 Regulated release from MMC .....                                  | 48 |
| 5.4 <i>In vitro</i> drug release of APIs reaching supersaturation ..... | 54 |
| 6. Summary and Conclusions .....  | 56 |
| 7. Future work .....  | 57 |
| 8. Svensk sammanfattning .....  | 58 |
| 9. Acknowledgements .....   | 60 |
| References .....  | 62 |

# 1. Introduction

Oral drug administration is considered to be the most convenient and preferred route because of its ease of administration and low costs, and because it is associated with high patient compliance. However, the successful performance and pharmacological activity of the drug compound is heavily reliant on its bioavailability. Several factors, such as aqueous solubility, dissolution rate, intestinal permeation and metabolism, could affect the oral bioavailability; the most frequent reason for low oral bioavailability is poor solubility [1, 2].

Since approximately 60% of the human body is made up of water, the aqueous solubility of a drug is a fundamental property that plays a major role in its absorption after oral administration. A specific concentration of the drug in the systemic circulation is required to achieve the desired therapeutic effect. Unfortunately, high doses of poorly water-soluble drugs are required in order to reach therapeutic plasma concentrations after oral administration, and this will increase the occurrence of side effects at the same time [3].

In general, it is believed that compounds with poor aqueous solubility will have limited oral bioavailability, and thus will fail in preclinical development. The improvement of drug solubility, and subsequently of oral bioavailability, is one of the most challenging aspects of drug development, especially for oral drug-delivery systems (DDSs). Numerous approaches have been reported to improve the apparent aqueous solubility of these drugs, including particle size reduction [4], solid dispersion [5-7], amorphous drug formulations and so on [8, 9]. However, because of high costs and mostly insignificant enhancement of solubility, these methods have been restricted and unsatisfactory.

In the last 20 years, scientists have been motivated to develop novel materials for poorly water-soluble drug delivery. Mesoporous materials have been proposed as a potential candidate for improving the solubility and bioavailability for these poorly water-soluble drugs [10, 11].

Porous materials are widely available and play a significant role in many aspects of our daily lives. There is a lot of empty space in the molecular structure of porous materials in comparison with nonporous materials, and thus porous materials have comparatively low density, large specific surface area, high free space volumes (pore volumes), and good energy absorption properties (heat exchange and insulation). Because of their different properties and parameters, porous materials have been used in various applications,

including catalysis, adsorption, separation, energy storage and tissue engineering [12-16].

One of the families of porous materials, mesoporous silica, has been widely studied because of its large internal surface area and tunable pores. The first document referring to a porous silica analogue was published in 1969; however, the authors only used “low-bulk density silica” to describe it because of the lack of detailed characterisation [17]. In 1992, the synthesis of ordered mesoporous molecular sieves was reported [18] and, in 2001, MCM-41 was first proposed as a drug carrier [10]. Since then, silica-based materials such as SBA-15 have been studied as DDSs [19-22] because the drug molecules can be loaded into and released from their pores. However, until recently, the main methods of synthesis of mesoporous silica materials have still relied on the use of organic surfactants as templates to form pores [18, 23-26].

This thesis introduces a new mesoporous material - mesoporous magnesium carbonate (MMC) - with a template-free synthetic process.

Developments in chemical synthesis over the last century have led to the production of a vast number of potential drug candidates; however, during this period, more and more poorly water-soluble drugs have also been introduced. Thus, increasing the dissolution rates of poorly water-soluble drugs has been an ongoing challenge for pharmaceutical scientists [27, 28].

The main goals of this body of research have been, firstly, to synthesise materials with a large surface area and controllable pore size using a template-free process; and, secondly, to use these porous materials as drug carriers with the aim of increasing the speed of release of poorly water-soluble drugs.

## 2. Aims of the thesis

The overall aim of this thesis was to investigate the application of MMC as a drug-delivery vehicle that would aid the solubility enhancement of poorly aqueous-soluble active pharmaceutical ingredients (APIs). In addition, the aim was to develop and improve understanding of the mechanism behind the formation of the mesoporous structure in MMC.

In more detail, the aims of each appended paper were to:

**Paper I:** Investigate the ability of MMC to enhance the stability of the amorphous forms of drugs with limited aqueous solubility, and thus improve their solubility. Ibuprofen was used as a model substance.

**Paper II:** Investigate the drug-release properties of MMC and its capacity for controlling the API release rate.

**Paper III:** Investigate the formation of the mesoporous structure and the possibility of controlling the pore diameter in MMC. The release of itraconazole from samples with different pore sizes was investigated *in vitro*.

**Paper IV:** Investigate the general applicability of MMC as a DDS for poorly water-soluble compounds with different proteolytic functions.

**Paper V:** Investigate the ability of MMC to control the API release rate via functionalising the surface of the MMC.

## 3. Background

### 3.1 Drug dissolution and bioavailability

The bioavailability of the API is a key factor to be addressed during formulation development of drugs intended for oral administration. The bioavailability of an API is the extent to which it is absorbed into the bloodstream and is thus able to trigger a therapeutic action (Figure 1). This characteristic is influenced by a complex chain of events, such as dissolution, absorption through the gastrointestinal wall, and liver metabolism [29]. Accordingly, poor solubility in the gastrointestinal tract can drastically limit the ability of an API to cause the desired therapeutic effect.

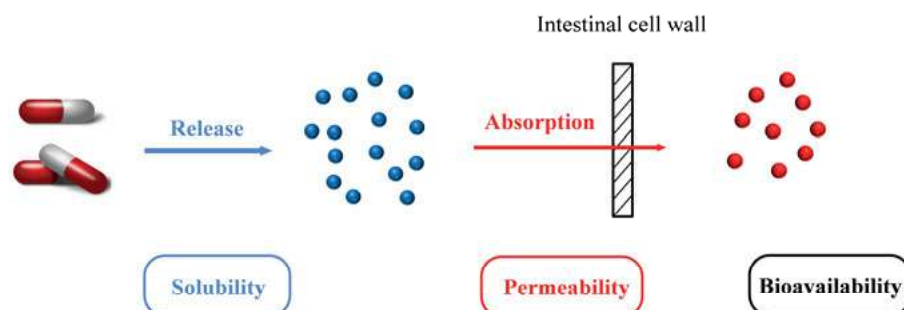


Figure 1. Sketch of API release and absorption leading to bioavailability.

The Biopharmaceutics Classification System (BCS) categorises drugs into four classes based on the solubility and membrane permeability of the APIs (Figure 2) [3, 30, 31]:

Class I (BCS I, drugs with both high solubility and high permeability): these drugs dissolve fast and instantly reach their target in the body;

Class II (BCS II, drugs with low solubility and high permeability): these drugs easily permeate the relevant physiological barriers but are poorly soluble in an aqueous medium;

Class III (BCS III, drugs with low permeability and high solubility): these drugs are soluble in the body; however, they permeate membranes poorly and cannot be taken up by the body;



Class IV (BCS IV, drugs with low permeability and low solubility): these drugs can neither dissolve in aqueous media nor permeate physiological barriers.

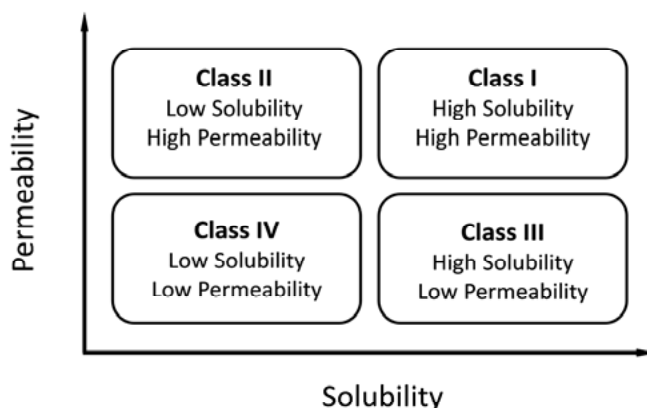


Figure 2. Biopharmaceutics Classification System (BCS).

Table 1 provides a list of solubility terms used in the United States Pharmacopeia (USP), including the terms very slightly soluble and practically insoluble which are used to describe drugs with the solubility lower than 1 mg/ml. However, in this thesis, these drugs (i.e. with the solubility lower than 1mg/ml) are referred to as poorly soluble [32].

Table 1. Solubility definition in the USP [32].

| Solubility definition | Parts of solvent required for one part of solute | Solubility range (mg/ml) |
|-----------------------|--|--------------------------|
| Very soluble          | <1   | >1000                    |
| Freely soluble        | From 1 to 10                                     | 100-1000                 |
| Soluble               | From 10 to 30                                    | 33-100                   |
| Sparingly soluble     | From 30 to 100                                   | 10-33                    |
| Slightly soluble      | From 100 to 1000                                 | 1-10                     |
| Very slightly soluble | From 1000 to 10000                               | 0.1-1                    |
| Practically insoluble | >10000   | <0.1                     |

Drug molecules are absorbed into, distributed and metabolised within, and excreted from our bodies, and the concept of bioavailability was introduced to describe “the relative amount of an administered dose that reaches the general circulation and the rate at which this occurs” [33]. In short, bioavail-

ability describes how much drug is effectively absorbed by our bodies. However, poor solubility of a drug in the intestinal fluid can result in low intestinal concentrations of the dissolved API [34] and, hence, low plasma concentration after oral administration. As the result, the desired therapeutic effect of the API will be very low or even non-existent.

## 3.2 Formulation procedures for enhancing the solubility of poorly water-soluble drugs

Insufficient bioavailability as a result of the limited solubility and low dissolution rate of poorly water-soluble drugs is especially common for BCS II (low solubility, high permeability) substances. Over the last decade, drugs that belong to BCS II have become more important because of advances in organic synthetic chemistry, which have led to the production of a vast number of potential drug candidates, as well as introducing more poorly water-soluble drugs into the pharmaceutical pipeline. It has been estimated that more than 40% of marketed drugs are poorly water-soluble and about 70% of all new APIs emerging from the discovery pipelines of pharma companies have poor aqueous solubility [6, 35, 36].

Unlike BCS IV APIs, where both poor solubility and poor permeability limit bioavailability, the bioavailability of a BCS II drug is only limited by its dissolution rate, and a small increase in dissolution rate can sometimes result in a large increase in bioavailability [2]. Therefore, enhancement of the dissolution rate of a drug is thought to be a key factor in improving the bioavailability of BCS II drugs. Five BCS II drugs were used as models in this thesis to study the effects of using MMC as a carrier on their solubility and dissolution rates.

Several physicochemical factors control the dissolution rate of a drug. According to the Noyes-Whitney equation (described in 3.2.2), increasing the saturation solubility and the effective surface area can have a positive impact on the dissolution rate. These factors can be affected through preformulation study and formulation design. Several methods, such as crystal modification, particle-size reduction, self-emulsification, pH modification, and amorphisation, are considered to be effective in improving the dissolution rates of BCS II drugs. This section discusses a number of different formulation strategies that have been reported in the literature to improve the solubility of poorly soluble drugs. These strategies are categorised into chemical and physical techniques.

## 3.2.1 Chemical methods

### 3.2.1.1 Crystalline salt forms

Crystalline salt forms of weak acid or basic compounds often have higher dissolution rates and normally are more soluble in aqueous media than their corresponding acids or bases [37, 38].

Although using a salt form is a common approach for enhancing the solubility and increasing the dissolution rate of an oral solid dosage form, there is still risk of unwanted or unexpected side effects (Table 3). Many medical therapies fail to achieve the desired outcomes because of patient non-compliance, and side effects are one of the main reasons for this. For example, the formed salts may convert to the respective acid or base forms in the bloodstream or gastrointestinal tract, since blood is a very efficient basic buffer (pH 7.4), and this can result in the drug potentially precipitating at the injection site, leading to issues such as haemolysis, phlebitis, and potential changes in drug distribution [39].

Table 2. Possible advantages and disadvantages of salt formulations [40].

| <b>Advantages</b>                | <b>Disadvantages</b>           |
|----------------------------------|--------------------------------|
| Enhanced solubility              | Increased hygroscopicity       |
| Increased dissolution rate       | Decreased chemical stability   |
| Higher melting point             | Corrosiveness                  |
| Improved photostability          | Possible disproportionation    |
| Higher bioavailability           | Additional manufacturing steps |
| Better processability            | Increased toxicity             |
| Easier synthesis or purification |                                |
| Potential for controlled release |                                |

### 3.2.1.2 Prodrugs

Prodrug design, or chemical modification of the molecular structure, is a widely known strategy that aims to modulate the biophysics and pharmacokinetic properties of drugs to improve their solubility, dissolution rate and pharmacokinetic features. Normally, prodrugs are inactive, bioreversible derivatives of active drug molecules that must undergo an enzymatic and/or chemical transformation in the body to metabolise into the active parent drugs (Figure 4), which can then exert their pharmacological actions in the body [41-43].

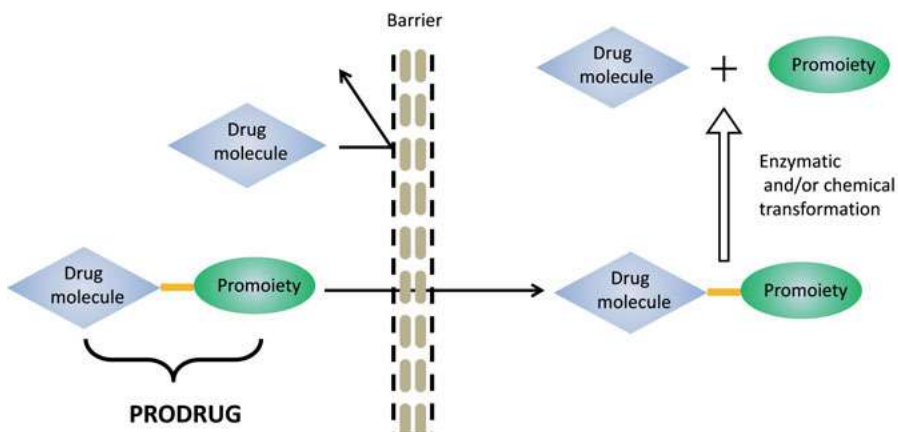


Figure 3. A simplified illustration of the prodrug concept.

In most cases, prodrugs are chemical derivatives that are only one or two chemical or enzymatic steps away from the active parent drug; however, some drugs lack an obvious carrier or promoiety. Although the prodrug approach is a feasible way of improving the erratic properties of investigational drugs or drugs already on the market, the development of a prodrug may still be very challenging.

### 3.2.2 Physical methods

Several factors can affect the dissolution rates of solids, as described by the Noyes-Whitney equation. This theory, proposed in 1897, discusses diffusion-controlled dissolution and involves no chemical reaction:

$$\frac{dm}{dt} = \frac{AD(C_s - C_d)}{d}$$

where  $dm/dt$  is the dissolution rate of a drug,  $A$  is the available surface area of the dissolving solid,  $D$  is the diffusion coefficient of the drug in solution,  $C_s$  is the saturation solubility of the drug in solution,  $C_d$  is the concentration in the bulk solvent/solution and  $d$  is the thickness of the diffusion layer of the dissolving substance.

In this equation model,  $C_s$  is the saturation concentration of the solute in the given solvent. The intrinsic dissolution rate is the dissolution rate of a pure solute, normalised to the solute surface area; normally, the dissolution rate decreases with time.

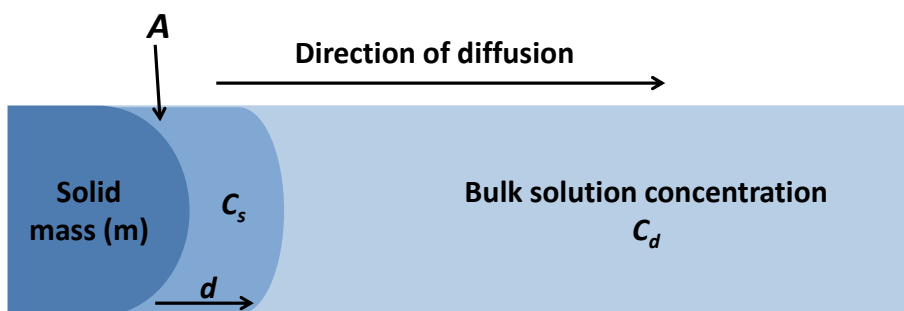


Figure 4. Noyes-Whitney parameters for dissolution rate.

Each parameter in the Noyes-Whitney equation is dependent on many factors that affect the dissolution rate of the drug. These factors are summarised in Table 3.

Table 3. Physicochemical factors affecting the drug dissolution rate.

| Term in the Noyes-Whitney equation                                   | Affected physicochemical parameter             |
|--|--|
| $A$ , surface area of solute solid                                   | Size of solid particles                        |
| $C_s$ , saturation solubility of solute in solution                  | Temperature                                    |
|  | Nature of dissolution medium                   |
|  | Molecular structure of solute                  |
| $C_d$ , concentration of solute in solution                          | Crystalline form of solid                      |
|  | Volume of dissolution medium                   |
| $D$ , diffusion coefficient<br>$d$ , thickness of the boundary layer | Remove dissolved solute from the dissolution   |
|  | Degree of agitation, such as speed of stirring |
|  | Volume of dissolution medium                   |
|  | Viscosity of dissolution medium                |
|  | Nature of diffusing molecules                  |

The Noyes-Whitney equation explains how certain factors affect the rate of mass transfer of solute particles into a solvent. Numerous physical formulation methods are based on the Noyes-Whitney equation, including those that physically modify the APIs. A summary of existing approaches [5] to improve the solubility and/or increase the dissolution rate is presented in Table 4. According to the Noyes-Whitney equation, the possible strategies for improving the solubility and/or dissolution of an API are: i) increasing the valid surface area for dissolution by decreasing the particle size of the compound, ii) optimising the wetting characteristics of the compound surface in order to

decrease the boundary layer thickness, and iii) improving the apparent solubility of the drug under physiologically relevant conditions.

Table 4. Approaches for improving the solubility and/or dissolution rate.

---

| <b>Physical modification</b>      |
|-----------------------------------|
| Particle size                     |
| Micronisation                     |
| Nanosuspensions                   |
| Crystal modification              |
| Polymorphs                        |
| Complexation/solubilisation       |
| Use of surfactants                |
| Use of cyclodextrins              |
| Drug dispersion in carriers       |
| Solid dispersions (non-molecular) |
| Solid solutions                   |
| Eutectic mixtures                 |

---

### **3.2.2.1 Particle-size reduction**

Particle-size reduction is a well-studied strategy for improving the solubility of drugs. Several methods have been reported for production of nanosized drug particles, including spray drying, homogenisation, microfluidation and milling [44, 45]. Irrespective of the approach taken to generate drug nanoparticles, the surface area will be increased significantly in comparison to particulates greater than 1 micron (Figure 5) and therefore the dissolution rate will be increased [46]. However, this tremendous increase in surface energy can cause the nano-sized drug particles to spontaneously aggregate into a more thermodynamically stable state [47].

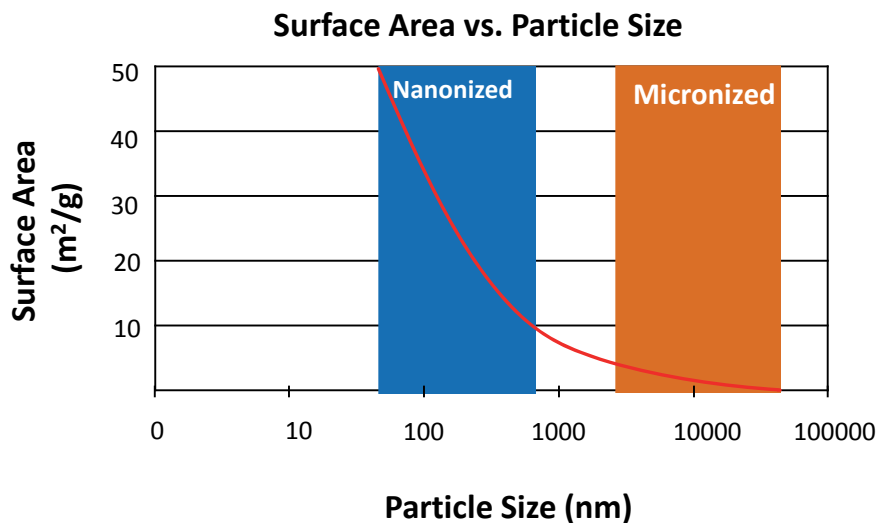
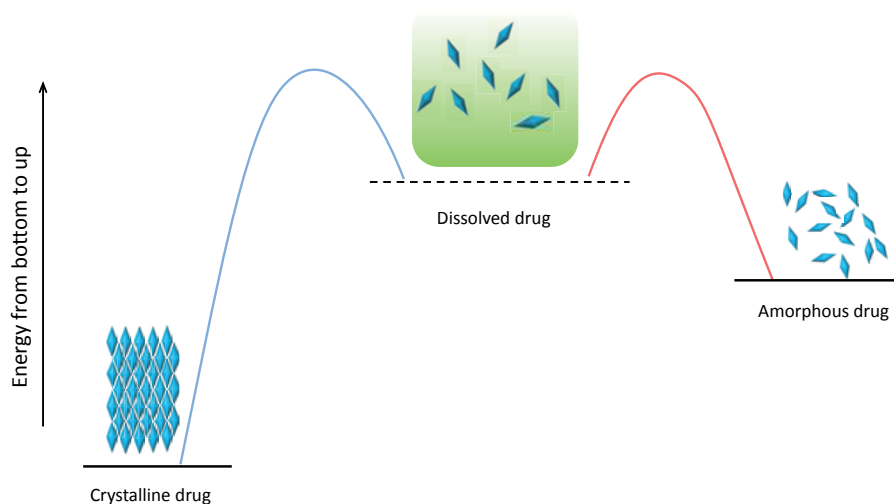


Figure 5. Demonstration of the increase in surface area when solids are modified from the micron size range to nano-sized particles; the red line is the surface area.

### 3.2.2.2 Crystal modification

As a structured solid state, a compound can exist as different crystalline forms (i.e. polymorphs). Compounds that lack crystalline characteristics are referred to as amorphous.

Molecular interactions within a crystal lattice include van der Waals forces, hydrogen bonding,  $\pi$ - $\pi$  interactions, electrostatic interactions and ionic interactions. The sum of the energies from all intermolecular interactions determines the total packing energy of the crystal. Stronger intermolecular interactions could result in lower mobility of the molecules within the crystal; and higher crystal energy could increase the stability of a crystal, but decrease the dissolution rate at the same time (Figure 6).



*Figure 6.* Illustration of the energy state comparison between amorphous and crystalline states of an API.

Here, an understanding of the distinction between solubility and dissolution should be provided. The solubility, or thermodynamic solubility (which is a thermodynamic property), is the equilibrium solubility of a compound, defined as the maximum quantity of that substance which can be completely dissolved at a given temperature and pressure in a given amount of solvent. The solubility presents how much of a compound is able to dissolve in a solvent; it has nothing to do with the time. In contrast, the dissolution rate (an important kinetic property) is an indication of whether the dissolution process is fast or slow. The dissolution rate strongly depends on the crystal form; and different polymorphs of the same molecule can have different dissolution rates.

Crystal modification can increase the dissolution rate, but cannot change the solubility; given sufficient time, the undissolved solute will convert to the most stable polymorph and the dissolution characteristic will approach the solubility (Figure 7). Therefore, the dissolution rate can be improved by crystal engineering; however, improving the solubility requires chemical modification of the structure of the drug molecule.



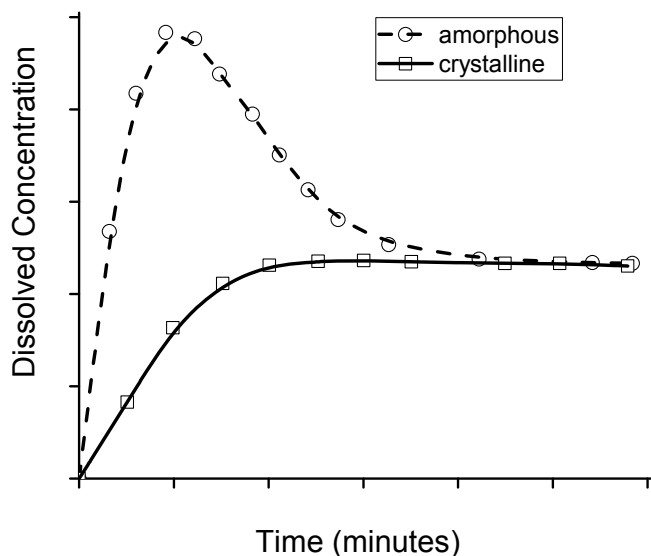


*Figure 7.* Illustration of the dissolution profiles of amorphous and crystalline state of an API.

For drugs with low aqueous solubility, the crystal form can be crucial to the performance of the dosage form. The bioavailability of water-insoluble compounds that need to be given orally in high doses can be highly affected by the physical form of the compound. An alternative approach to the enhancement of solubility, dissolution and bioavailability is through the application of crystal modification. The physicochemical and bulk material properties of the API can be modified, whilst maintaining the intrinsic activity of the drug molecule. The use of polymorphs and amorphous forms is a very well known strategy in crystal modification methods.

#### *3.2.2.2.1 Polymorphs*

Polymorphism is often defined as the ability of a substance to exist as two or more crystalline phases that have different arrangements and/or conformations of the molecules in the crystal lattice. If the crystallisation conditions are changed, it is possible that the molecules may start to form crystals with different packing patterns which have different crystal energies. The form with the lowest free energy is the most stable structure and this will have the highest lattice energy and melting point. Other less stable forms with higher free energy are described as metastable states; these have different properties, such as density and melting point.

Generally, there is a relationship between the melting points of the different polymorphs and the dissolution rates:

High melting point = strong crystal lattice = low molecular mobility = low dissolution rate

Accordingly, the form with the highest melting point will have the slowest dissolution rate.

### 3.2.2.2 Amorphous state

Unlike polymorphs, the arrangement of the molecules in an amorphous solid is irregular (Figure 8), and that is why amorphous solids have poorly defined patterns when exposed to powder X-ray diffraction (XRD) analysis. The energy states of amorphous solids are much higher than those of the crystal forms. If an amorphous solid is maintained at a specific temperature for a long period, the component molecules or atoms gradually rearrange into a more highly ordered crystalline form (low energy state).

Because of the irregular arrangement, amorphous solids usually have very different properties from those of the crystal form of the same material. For example, compared with the distinct melting point of a crystal, amorphous solids tend to soften slowly over a wide temperature range, as there is no crystal lattice to break in the amorphous state.

Due to the high energy state and no crystal lattice barrier, amorphous solids have higher dissolution rates than the crystal forms. However, because they have the same molecular structure, amorphous solids have the same clinical effects as the crystal forms.

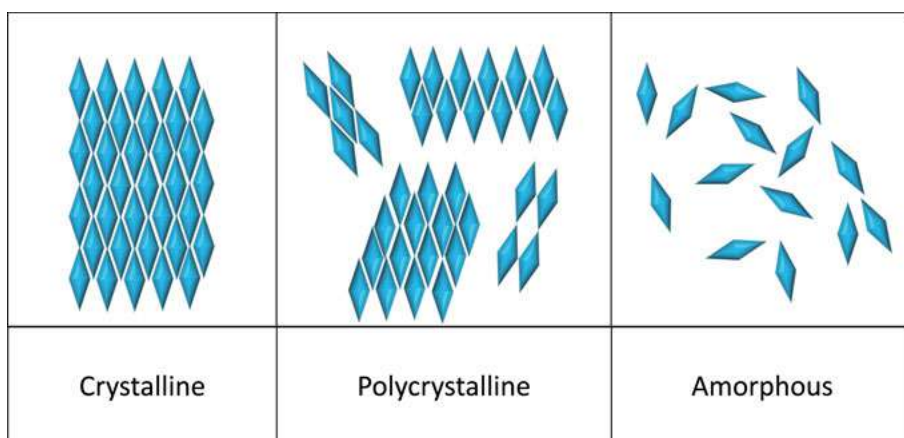


Figure 8. Classification of the physical states of drug molecules.

When a metastable form is dissolved, it can result in more material in solution than seen with a saturated solution of the more stable form, which means that the amorphous form can dissolve to give a supersaturated solution. These supersaturated solutions will eventually return to the equilibrium solubility, as the stable crystal form precipitates from the solution, but this

process may not be instantaneous. In fact, the supersaturated solution can often exist long enough to increase the bioavailability of a poorly soluble drug (Figure 7).

Because a metastable state can return to its stable state, a drug component in an amorphous state is able to recrystallise (Figure 9). Maintaining this component, such as a poorly water-soluble drug, in its amorphous state is one of the great challenges in the pharmaceutical industry.

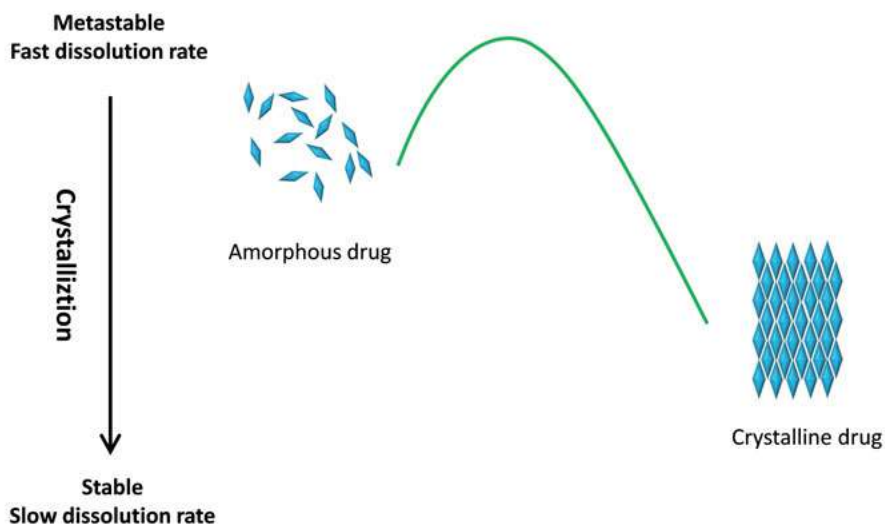


Figure 9. Illustration of crystallisation from amorphous drug to crystalline drug.

### 3.3 Approaches to stabilise an amorphous solid

Because the amorphous form of a drug has high free energy and therefore higher dissolution rate than the crystal form, there is an opportunity for overcoming dissolution-limited absorption and bioavailability challenges. However, because of the high free energy, the amorphous form is thermodynamically unstable, and thus pure amorphous drugs are rarely developed alone as pharmaceutical products. This has encouraged investigation into the stabilisation of molecules in the amorphous physical state.

In the last decade, development of amorphous solid-dispersion formulations/methods for stabilising amorphous molecules has created tremendous opportunities for the pharmaceutical scientist to address issues relating to the bioavailability of poorly soluble molecules, such as using polymers and surfactants as excipients to prepare and stabilise the amorphous form of a drug. Recently, it has been found that after incorporating the amorphous drug into the porous structure such as mesoporous material, crystallisation can be inhibited. Porous materials have thus expanded the opportunities for pharma-

ceutical scientists to establish new stabilisation strategies for amorphous formulations.

### 3.3.1 Polymers

The use of a polymer matrix as an excipient is one of the most common methods for stabilising nano-sized drug particles or amorphous API states [48]. Table 5 lists examples of commercial polymers. By increasing the glass transition temperature ( $T_g$ ), polymers improve the physical stability of the amorphous compounds and delay their crystallisation. Many papers have reported that a hydrophilic polymer carrier matrix (for example, polyvinylpyrrolidone, polyethylene glycol, hydroxypropyl methylcellulose and some cellulose derivatives) can significantly alter the dissolution behaviour and stability of hydrophobic drugs [49-51].

Recent studies have found that, in some polymeric formulations, polymer matrices not only stabilise the dispersed amorphous drug but also increase its wettability and prevent the drug from precipitating in the stomach and intestine [52, 53].

Table 5. Examples of commercially available polymers in solid dispersions [54].

| <b>Brand name</b> | <b>Drug</b>  | <b>Polymer used</b> |
|-------------------|--------------|---------------------|
| Gris-PEG          | Griseofulvin | PEG                 |
| Sporanox          | Itraconazole | HPMC                |
| Rezulin           | Troglitazone | PVP                 |

HPMC, hydroxypropyl methylcellulose; PVP, polyvinylpyrrolidone; PEG, polyethylene glycol.

### 3.3.2 Surfactants

Usually, surfactants are organic molecules that have two distinct parts of their chemical structures. One part is hydrophilic and the other is hydrophobic. Because of their amphiphilic properties, surfactants can be found at the interfaces between two phases, such as water-air or water-oil interfaces [55].

In some cases, it has been suggested that the addition of surfactants into formulations containing an amorphous drug may affect nucleation by either changing the viscosity of the molecule (and therefore affecting the kinetic barrier to crystallisation) or modifying the interfacial energy at the amorphous solid interface. Further, there is also the possibility that surfactants related to the product, that are adsorbed at the interfaces of molecular clusters, can inhibit crystal growth [56-59]. However, the capacity for surfactants to stabilise amorphous APIs depends on many and various factors, such as the chemical structures of the drug and the surfactant, the polarity of the drug, the temperature and the pH value.

### 3.3.3 Porous materials/Mesoporous materials

Porous materials are materials containing pores (voids, cavities, channels or interstices). According to the IUPAC definition, materials with pore widths not exceeding 2 nm are defined as microporous materials, materials with pore widths exceeding 50 nm are defined as macroporous materials and materials with pores between 2 nm and 50 nm are defined as mesoporous materials [60]. Zeolites and mesoporous silica are the most famous of the porous materials (Figure 10).

Zeolite was first discovered in 1756 by the Swedish scientist Axel Cronstedt. In the 1930s, scientists found that zeolites could act like sieves because they could separate molecules [61]. More precisely, zeolites are crystalline, with a defined microporous structure that contains molecular-sized pores and large internal voids [62, 63].

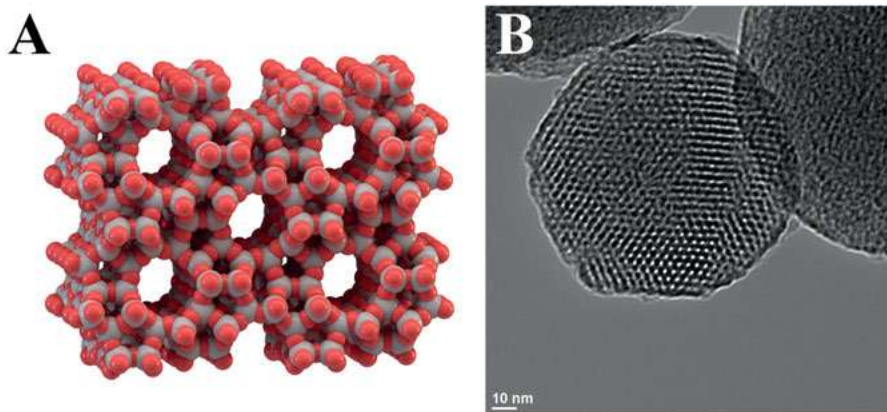


*Figure 10.* A) Schematic image of zeolite (ZSM-5, image courtesy of Thomas Splettstoesser); B) TEM image of mesoporous silica (image courtesy of Dr. Victor Shang-Yi Lin).

The use of mesoporous materials such as MCM-41 and SBA-15 as DDSs to maintain the amorphous form of drugs has been well studied [10, 11, 64-67]. Recently, several studies have shown that amorphous drugs may stay in the amorphous state after being incorporated into mesoporous materials [68-71]. For example, when the co-spray drying method was used to incorporate amorphous ibuprofen in mesoporous SBA-15 [71] it was shown that the nano-scaled mesoporous channels entrapped the amorphous ibuprofen molecules with resultant excellent physical stabilisation under severe storage conditions. However, other works have reported that crystallisation can occur in mesoporous materials with larger pore size ( $> 20$  nm) [70]. There are two reasons for the ability of mesoporous materials to prevent the crystallisation of incorporated amorphous ibuprofen: lower molecular mobility and limited space for crystal growth. It has been observed that there is a correla-

tion between molecular mobility and stability in many amorphous drugs [72, 73]. The physical stability often improves when the molecular mobility is reduced. The molecular mobility of ibuprofen confined in nanostructured silica material, SBA-15, has been investigated using dielectric relaxation spectroscopy [74]. The results showed that ibuprofen molecules interacting with the pore walls had low mobility, and that this interaction between molecules at the pore walls and molecules of amorphous ibuprofen might have prevented the amorphous ibuprofen from crystallising, thereby yielding a stable amorphous drug. The other reason, limited space for crystallisation, is very easy to understand; when crystallisation occurs, enough space is needed for crystal growth - if the space is limited, crystallisation will be inhibited.

Mesoporous silica is another well-studied material in the family of mesoporous materials. By mid-2016, according to Web of Science, there had been more than 76,600 scientific papers published on mesoporous silica since the 1970s (search term: mesoporous silica). The synthesis of mesoporous silica was first reported in the early 1990s when surfactant micelles were used as a template [18, 23]. Since then, the template method has been widely applied to prepare mesoporous silica materials with high surface areas, tunable pore sizes and large pore volumes [75, 76].

Because of the high surface area, uniform pore size, and narrow pore-size distribution, mesoporous silica materials are interesting supports for organic functional groups [77-79]. The introduction of functional organic groups (functionalisation) into the mesoporous material permits regulation of the surface physical and chemical properties (e.g., hydrophobicity, hydrophilicity, acidity, alkalinity and binding to guest molecules), alteration of the surface reactivity, adjustment of the surface selectivity, and surface protection against chemical attack. Various literature reports have described methods of functionalising the interior pore surfaces of mesoporous solids such as MCM-41 and SBA-15 by incorporating organic and/or inorganic components either on the silica surface or trapped within the channels.

Functionalised mesoporous silica materials are of great interest because of their potentially wide applications in various areas, such as catalysis, adsorption/desorption, drug delivery, chromatography, nanotechnology, ion extraction, and imprinting for molecular recognition [16, 78-83]. For example, because mesoporous silica has thiol groups on the pore surface, heavy metal ions such as Hg, Ag, and Cd are potentially able to be adsorbed [84, 85]. Sulfonic acid groups grafted onto mesoporous materials, as another example, exhibit high catalytic activity for selective formation of bulky organic molecules [86].

## 3.4 Magnesium Carbonate

### 3.4.1 Magnesium Carbonate Minerals

Magnesium carbonate is an inorganic salt that is usually white-coloured. Since it is highly absorptive, magnesium carbonate is sometimes used to absorb odours [88]. Anhydrous magnesium carbonate is rarely found in nature. Hydrated forms of magnesium carbonate, such as nesquehonite ( $\text{MgCO}_3 \cdot 3\text{H}_2\text{O}$ ) (Figure 11) and lansfordite ( $\text{MgCO}_3 \cdot 5\text{H}_2\text{O}$ ), and a number of basic carbonate minerals, such as hydromagnesite ( $4\text{MgCO}_3 \cdot \text{Mg}(\text{OH})_2 \cdot 4\text{H}_2\text{O}$ ) and dypingite ( $4\text{MgCO}_3 \cdot \text{Mg}(\text{OH})_2 \cdot 5\text{H}_2\text{O}$ ), are probably the most common forms of the compound.

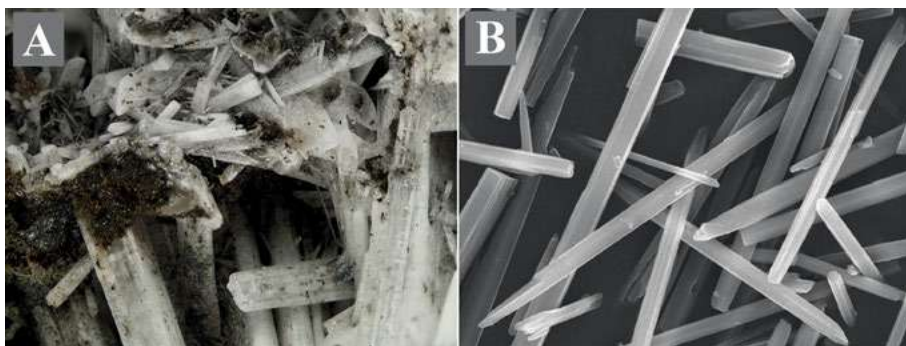


Figure 11. A) Photograph and B) scanning electron microscopy image of Nesquehonite ( $\text{MgCO}_3 \cdot 3\text{H}_2\text{O}$ ).

According to the U.S. Food and Drug Administration, magnesium carbonate and magnesium oxide generally recognized as safe (GRAS) and can be used in pharmaceutical formulations and as food additives [89]. In a pharmaceutical formulation application, magnesium carbonate is used as a tablet diluent/excipient in concentration up to 45 wt.% [88] because of its high crushing strength, low friability and good disintegration properties [90-92]. In tableting processes, magnesium carbonate is used to absorb liquids (such as flavours) and it is also added to numerous food products to prevent them from absorbing water in order to inhibit lump formation. Magnesium carbonate has also been incorporated in microsphere formulations for the purpose of stabilising encapsulated proteins [93] and is used as an ingredient in antacids [94].

### 3.4.2 Mesoporous Magnesium Carbonate (MMC)

It is easy to figure out from the name MMC that this material is magnesium carbonate with a mesoporous structure (pores between 2 and 50 nm in diameter, see Figure 12).

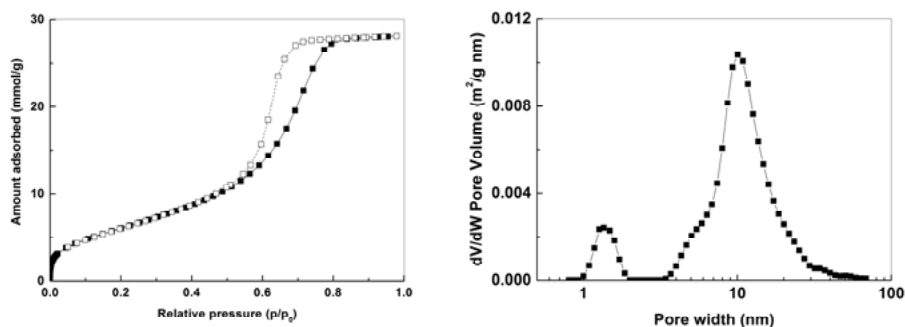


Figure 12. N<sub>2</sub> adsorption isotherms (left) and density functional theory (DFT) pore size distribution (right) of MMC.

In this thesis, however, unlike those well studied mesoporous silica materials which have unique pore structures, as clarified by transmission electron microscopy (TEM) images [18, 95-98], mesoporous magnesium carbonate has a non-traditional “pore structure” (this will be discussed in more detail in section 5). In other words, MMC does not have an ordered structure or uniform pore size. Instead, the mesoporous structure of MMC is the free space between the amorphous magnesium carbonate and magnesium oxide nanoparticle aggregations (Paper III).

MMC was first synthesised at the division of Nanotechnology and Functional Materials (NFM) at Uppsala University [87]. Its uniquely high surface area and well-defined mesoporous structure make MMC an interesting drug carrier candidate for stabilising the amorphous state of the incorporated APIs to improve solubility [99]. In this thesis work, MMC was investigated as a DDS with the potential to stabilise, and control the release of the amorphous forms of BCS II APIs, thus improving their dissolution rates and potentially their bioavailability.

### 3.4.3 Functionalisation of MMC

The usual method for post-synthesis functionalisation is by amine grafting using different aminosilanes [100]. It has been reported that grafting aminosilanes to the surface of a mesoporous material will change the drug loading and release profile of the material. For example, amine-modified SBA-15 nanoparticles showed enhanced loading capacity and prolonged release of the loaded drug [101, 102]. In this thesis, due to the low cost and high availability, (3-aminopropyl)triethoxysilane (APTES) was chosen as the aminosilane to functionalise (modify) the surface of MMC powder.

After revealing the nanostructure of MMC and achieving control of the average pore size of the material without templates or surfactants, continuing work is expected to further broaden the versatility of this material. Like mesoporous silica, MMC has the benefit of a high surface area, and can also



support organic functional groups (functionalisation). Functionalisation of MMC with interesting organic groups could allow the surface physical and chemical properties to be changed, thus altering its surface reactivity and selectivity, and new applications for this material will continue to emerge.

In this thesis, surface functionalisation of MMC was successfully carried out using APTES. It was found that amine grafting preferably occurred on the walls (surface) of the MMC pores. Later, ibuprofen was used to investigate APIs loading into and release from this modified form of MMC (m-MMC). The results showed that all the modified MMC materials were able to stabilise the amorphous phase of ibuprofen and that its release could be controlled by adjusting the amine surface coverage of MMC.

## 4. Methodology

A more detailed description of the methodology can be found in the “Materials and Methods” section in the individual publications.

### 4.1 MMC synthesis

In a typical synthesis, MgO (Sigma-Aldrich) was mixed with methanol (VWR) in proportions of 1:15 in a reaction vessel. The vessel was sealed and CO<sub>2</sub> (AirLiquide) was applied at pressure of 1 - 4 bar. The reaction mixture was left stirring for 24 - 72 h at 55 °C (Papers I and II) or room temperature (Papers III and V) and then the pressure was released. A cloudy, off-white solution was formed.

The solution was centrifuged (5000 rpm) for 30 - 60 min in order to remove unreacted MgO particles and an optically clear, yellow-coloured liquid was obtained (Papers III and V).

This liquid slowly formed an alcogel after it was evaporated in a ventilated environment and subsequently started to break up into wet particles. The small particles were dried in a vacuum oven at 75 °C (Papers I and II) or under a flow of nitrogen gas at 80 °C (Papers III and V) for minimum of 6 h.

The powder was then dried at 250 °C for 6 to 12 h to remove all remaining organic compounds and a white powder (Papers I and II) was formed. For the investigation into pore-size control (Paper III), the dried powder was first kept at 150 °C for 3 h and then at 250 °C overnight, both under N<sub>2</sub> flow (Papers III and V).

### 4.2 MMC modification

MMC was modified by grafting APTES to its surface under reflux. Prior to the experiment, all glassware was heated to 150 °C overnight to dry; the system was flushed with nitrogen gas during the experiment to maintain an inert atmosphere. The reactor was then securely sealed to prevent moist air from affecting the modification process.

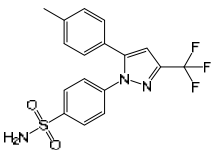
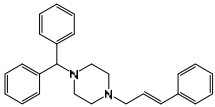
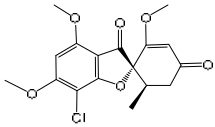
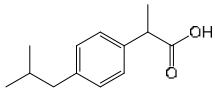
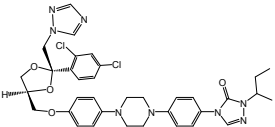
Firstly, in a three-necked round flask, MMC was dispersed in anhydrous toluene and then heated to 110 °C. When the temperature had stabilised, APTES was slowly added to the mixture, which was then refluxed. After

refluxing for 24 h, the mixture was cooled to room temperature and filtered to obtain m-MMC, which was then washed with ethanol and dried overnight at 70 °C in the oven (Paper V).

### 4.3 API loading method

The APIs were incorporated into MMC via soaking method: an amount of the API was dissolved in ethanol (Papers I, II, IV and V) or methylene chloride (Paper III) and then MMC was added to the solution. The mixture was placed on an orbital shaker at 100 - 300 rpm at room temperature for 24 h to allow for diffusion of the APIs into the MMC. Subsequently, the mixture was heated until evaporation of the solvent was complete, after which the drug-loaded sample was left to dry in the oven for 24 h. In this thesis, five BCS II compounds were studied; the oral absorption of these compounds is normally limited by their low solubility and/or dissolution rate (Table 6).

Table 6. Studied drugs, their molecular structures and melting points.

| API          | Abbreviation | Papers using the API | Melting point (°C) | Molecular structure  |
|--------------|--------------|----------------------|--------------------|--|
| Celecoxib    | CEL          | IV                   | 156                |   |
| Cinnarizine  | CIN          | IV                   | 118                |  |
| Griseofulvin | GRI          | IV                   | 220                |  |
| Ibuprofen    | IBU          | I, II and V          | 78                 |  |
| Itraconazole | ITZ          | III                  | 166                |  |

## 4.4 Materials characterisation

The MMC and drug-loaded samples in this thesis were analysed using various analytical techniques.

### 4.4.1 Powder X-ray diffraction (XRD)

XRD is used to characterise and identify the crystalline structure of a material. Here, XRD was used to investigate: i) the material structure and ii) the crystallinity of the APIs after they had been loaded into MMC.

In this work, the XRD patterns were recorded by a Bruker D8 Advance Twin-Twin instrument with Cu-K $\alpha$  radiation ( $\lambda = 1.54 \text{ \AA}$ ). The samples were ground manually prior to analysis and then placed in a zero-background silicon sample holder.

### 4.4.2 Scanning electron microscope (SEM)

The scanning electron microscope is the most widely used instrument in materials research and analysis. It can produce images by scanning the sample with a focused electron beam. The electrons interact with the atoms of the sample, providing information relating to its topographical features, morphology, phase distribution and compositional differences.

SEM in this thesis was used to study the morphology of the particles as well as their sizes. The SEM images (Papers I, II, III and V) were obtained using a LEO 1550 microscope (Zeiss) operating at a voltage of 0.5 - 2 kV, and all the samples were coated with a thin layer of gold prior to analysis. An in-lens detector was used to collect the secondary electron signals. Additional SEM images in Paper III were recorded using a Hitachi TM3000 table-top SEM instrument (Tokyo, Japan) operating at 15 kV.

### 4.4.3 Nitrogen adsorption/desorption isotherms

Nitrogen adsorption is the most practical method of determining the porosity of mesoporous materials. Textural information about a solid material, including surface area, pore volume and pore-size distribution, can be obtained by the adsorption of gases onto a porous solid at various relative pressures and fixed temperature.

In this work, an ASAP 2020 volumetric surface area analyser from Micromeritics was operated at 77 K to obtain information such as the Branauer-Emmet-Teller (BET) surface area (calculated in the relative pressure range of 0.05-0.30), the total pore volume (by single point adsorption at a relative pressure of 0.98) and the pore diameter distribution (calculated using the density functional theory (DFT) under slit geometry by N<sub>2</sub> model).

#### 4.4.4 Thermogravimetric analysis (TGA)

TGA measures weight/mass changes in a material as a function of temperature, or as a function of time (with constant temperature), under a controlled atmosphere. TGA analysis is performed by gradually raising the temperature of a sample (or maintaining a chosen temperature) in a furnace, while the sample is being weighed; any thermal event involving mass loss will be recorded. In this thesis, TGA analysis results were used to determine the amount of API loaded into MMC, as MgO is thermally stable under 900°C, while all the APIs will evaporate or decompose at temperatures below 600 °C.

The measurements were made using a MettlerToldeo TGA 2 instrument (Greifensee, Switzerland). The samples were heated in air from room temperature to higher than 600 °C with a heating rate of 3 - 5 °C/min.

#### 4.4.5 Differential scanning calorimetry (DSC)

DSC measures temperatures and heat flows associated with the thermal transitions occurring in a material. The difference in the amount of heat required while increasing the temperatures of the sample and the reference (which typically is just an empty sample pan) is measured as a function of temperature. When the sample undergoes a physical transformation, such as a phase transition (melting for example), DSC records the heat flows and thus the melting point can be determined.

In this thesis, DSC was used to determine the thermal properties of the loaded APIs. The experiments were carried out on a DSC Q2000 instrument from TA instruments (New Castle, Delaware, USA) using Exstar software. Samples of 3 - 6 mg were weighed into 5 mm aluminium pans and sealed. They were first cooled to -35 °C and then heated to 150 °C at a heating rate of 3 °C min<sup>-1</sup> (Papers I, II and V) or to 250 °C (Papers III and IV). The instrument was calibrated for the melting point and heat of fusion ( $T_m$  [°C] and  $\Delta H_m$  [mJ mg<sup>-1</sup>]) of indium (156.6 °C and 28.4 mJ mg<sup>-1</sup>).

#### 4.4.6 Dynamic light scattering (DLS)

DLS is used to determine the size of particles by measuring the changes in the intensity of light scattered through a suspension or solution. These changes are related to the sizes of the particles in the suspension or solution. Thus, it is possible to calculate the particle-size distribution and give a description of the particle motion in the medium.

In this work, DLS was used to investigate how the particles aggregated over time in the reaction solution by observing increases in the hydrodynamic radius of the particles. In Paper III, the size distribution of the particles was measured using a Malvern<sup>®</sup> Zetasizer Nano ZS (Malvern Instruments

Nordic AB, Sweden), equipped with a 633 nm He-Ne laser and operating at room temperature.

#### 4.4.7 Infrared spectroscopy (IR)

IR is a mostly used technique that is based on absorption spectroscopy. By absorption of IR light with the exact amount of energy, vibrations and rotations of molecules and groups can be excited. This absorption therefore is used to identify the groups thus to analysis the structure of the organic compounds.

Here, IR was used to study the physical and chemical properties of MMC, m-MMC and the API-loaded samples. The infrared spectra were obtained using a Varian 610-IR (Santa Clara, California, United States) equipped with a Specac Goldengate attenuated total reflection (ATR) accessory (Orpington, UK) with a diamond ATR element and KRS-5 lenses. The spectra (400 - 4000  $\text{cm}^{-1}$ ) were recorded at a resolution of 4  $\text{cm}^{-1}$  using an RT deuterated-triglycine sulphate (DTGS) detector. Sixty-four background spectra were recorded prior to analysis and the spectra of the samples were signal averages of 128 scans.

#### 4.5 Drug-release analysis

The release of the APIs from the MMC samples was measured as the dissolution profile of the API as it dissolved in a USP-II dissolution bath (Sotax AT7 Smart, Sotax AG, Switzerland) equipped with 1000 mL vessels (37 °C, 50 rpm). Drug-loaded samples were placed in vessels containing phosphate buffer at pH 6.8 (Papers I, II, IV and V) or simulated gastric fluid at pH 1.3 (Paper III). Aliquots of 3 mL were withdrawn from each vessel at regular intervals and the drug concentration in the liquid samples was analysed using UV/visual absorbance spectroscopy (UV-1800 Spectrophotometer, SHIMADZU, Japan). Measurements were made in triplicate. The dissolution of both pure drug crystals and API-loaded samples was assessed, and the mean concentration values and corresponding standard deviations were calculated.

## 5. Results and Discussion

### 5.1 Synthesis, structure and pore-size control of MMC

In paper III, MMC was found to be constructed from aggregated nano-sized MgO crystals (coated with amorphous MgCO<sub>3</sub>) and amorphous MgCO<sub>3</sub> nanoparticles. These aggregated nanocrystals and nanoparticles were adhered together by amorphous MgCO<sub>3</sub>. The pore size of MMC was adjusted by altering the energy input during the powder formation step during synthesis.

#### 5.1.1 Structural characterisation of MMC

The reaction between MgO and methanol under CO<sub>2</sub> pressure resulted in a coarse, white powder (MMC, Papers I, II and IV). The material was composed of MgCO<sub>3</sub> and unreacted MgO; the MgCO<sub>3</sub> was amorphous and the MgO was crystalline. Figure 13A shows the XRD pattern for MMC; the peaks correspond to the unreacted MgO.

The material formed after removal of unreacted MgO by centrifugation (c-MMC, Paper III), was optically transparent and XRD amorphous (Figure 13B).

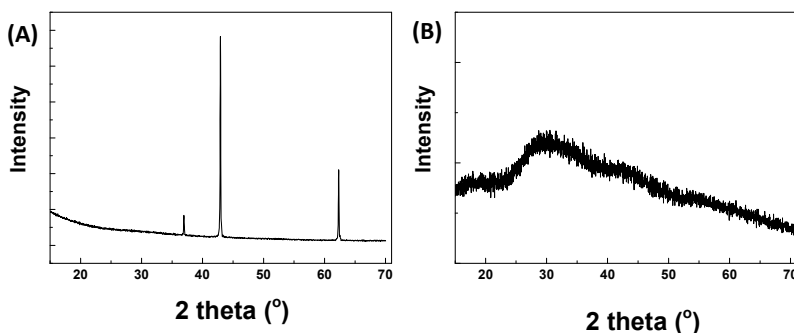


Figure 13. XRD patterns for: (A) MMC, the peaks at  $\sim 37^\circ$ ,  $\sim 43^\circ$  and  $\sim 62^\circ$  correspond to the unreacted MgO in the MMC; (B) c-MMC, without crystalline MgO peaks after centrifugation.

However, CHN elemental analysis and inductively coupled plasma optical emission spectrometry (ICP-OES) indicated that c-MMC still contained

about 14-18 wt.% MgO (Table 7). This was also confirmed by TGA analysis, which found that the oxide content was about 13.8 wt.%.

Table 7. Elemental composition and MgO content of c-MMC.

|      | C     | H    | N     | Mg   | MgO<br>(from CHN/ICP) | MgO<br>(from TGA) |
|------|-------|------|-------|------|-----------------------|-------------------|
| wt.% | 10.80 | 0.28 | <0.01 | 26.2 | 17.6                  | 13.8              |

High resolution TEM (HRTEM) images of the c-MMC sample showed that the material was composed of randomly oriented crystalline nanoparticles, about 2-5 nm in size, encapsulated by amorphous MgCO<sub>3</sub> forming clusters of about 30 nm in size (Figure 14(b) and (c)). The crystalline nanoparticles showed a ring-like Fourier transform pattern (Figure 14(d)) where the *d*-spacing of the crystals was in agreement with the *d*-spacing of MgO (0.219 nm and 0.153 nm, corresponding to the (200) and (220) planes, respectively). To simplify the discussion in this thesis, we refer to nanoparticles of around 2-5 nm as **Type I** nanoparticles and those of around 30 nm as **Type II** nanoparticles. The relationship between **Type I** and **Type II** nanoparticles is demonstrated in Figure 15. The TEM image (Figure 14 (e)) shows that a particle of MMC is made from aggregates of **Type II** nanoparticles. A possible process can be imagined where, after methanol was evaporated from the reaction mixture, these aggregated nanoparticles were fixed in place, possibly because of the precipitated amorphous MgCO<sub>3</sub> layer forming from the reaction mixture during methanol drying (as illustrated by Figure 18).

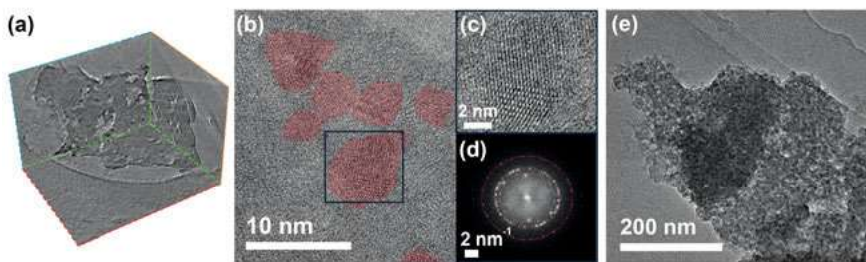


Figure 14. (a) 3D-orthoslice representation of the reconstructed tomogram of c-MMC; (b) HRTEM image of a c-MMC particle showing randomly oriented MgO nanocrystals surrounded by an amorphous layer; the crystalline parts are highlighted in red; (c) An enlarged view of an MgO nanocrystal marked in panel (b); (d) Fourier transform derivation of the HRTEM image in panel (b) with the rings (marked) corresponding to MgO; (e) TEM image showing the aggregated nanoparticles.



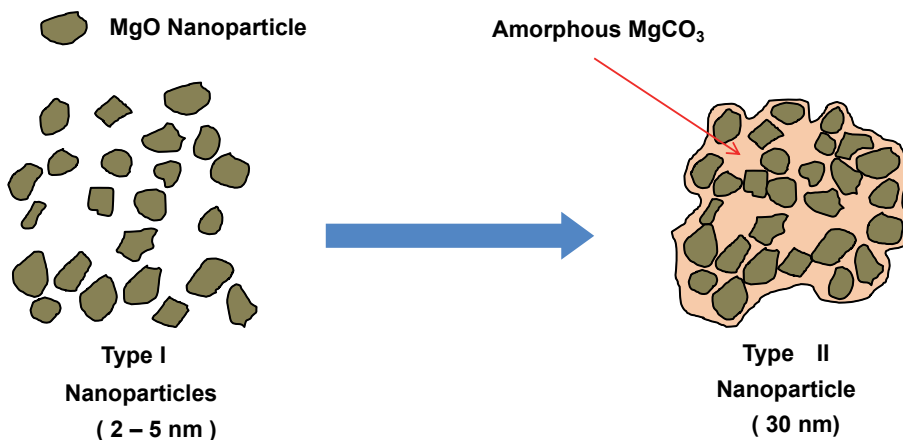


Figure 15. Schematic sketch of the formation of Type II nanoparticles from the aggregation of Type I nanoparticles.

DLS was used to follow the formation of the nanoparticles during the gelation of c-MMC (Figure 16). To start with, nanoparticles of  $\sim 50 - 100$  nm in diameter were detected in the optically clear reaction mixture. Significant growth of these particles occurred with time when the reaction mixture was covered and left standing at room temperature (i.e. without active evaporation/drying). After 150 minutes, the nanoparticles became too large to be detected by DLS, indicating the formation of MgO or MgO/MgCO<sub>3</sub> composite particles. Figure 15 illustrates the formation of **Type II** particles. However, DLS did not show the **Type I** nanocrystals, probably because of the fast aggregation from **Type I** to **Type II** nanoparticles, as described above.

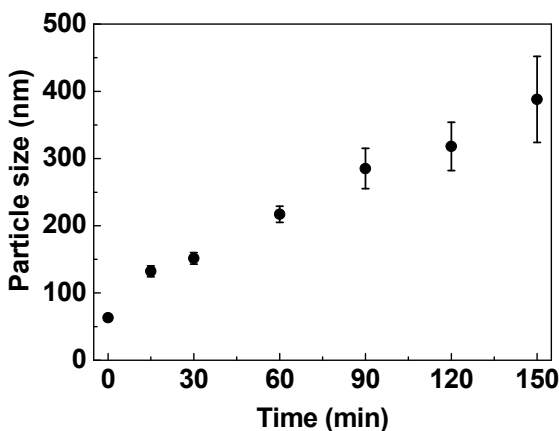


Figure 16. Particle diameter measurement as followed by DLS.

The SEM images (Figure 17) show the presence of **Type II** particles, and illustrate how they could have aggregated to form MMC particles. Macroscopically, a typical MMC particle appears to be smooth on the surface (Figure 17(a)), but at higher magnifications it can be seen that the surface is made of particles that aggregate (Figure 17 (b – d)). The packing of these **Type II** particles appeared to be unordered but it is important to note that the images were in agreement with the tilt series TEM images (Paper III). However, we could not draw any conclusions about the real morphologies of these **Type II** nanoparticles due to the thin gold layer coating applied on the SEM samples prior to analysis to avoid charging.

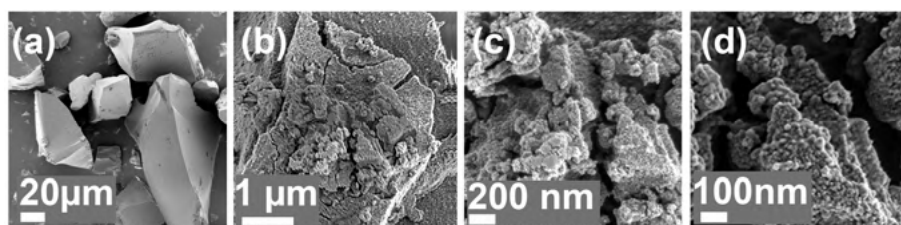


Figure 17. (a-d) Scanning electron microscopy images of a transparent c-MMC particle under different magnifications.

### 5.1.2 Pore-size control in MMC

The pore-size distributions in the c-MMC samples synthesised using different powder-forming conditions (outlined in Table 8) were obtained by DFT pore size analysis of N<sub>2</sub> sorption isotherms (Paper III).

Table 8. Powder formation temperatures, specific surface areas and pore properties of MMC samples.

| Samples  | A    | B    | C    | D <sup>b</sup> | E    | F    | G    |
|--|------|------|------|----------------|------|------|------|
| <b>Powder formation temperature (°C)<sup>a</sup></b> | -20  | 10   | 20   | 20             | 30   | 50   | 80   |
| <b>BET surface area (m<sup>2</sup>/g)</b>            | 263  | 497  | 499  | 173            | 618  | 661  | 690  |
| <b>Peak DFT pore size (nm)</b>                       | ~13  | ~10  | ~6.5 | ~20            | ~5.1 | ~3.4 | ~2.9 |
| <b>Total pore volume (cm<sup>3</sup>/g)</b>          | 1.27 | 1.15 | 0.97 | 1.00           | 0.76 | 0.60 | 0.50 |

a) Mechanical stirring was used to form the gel and powder for all samples except sample D.

b) No stirring during the powder formation process.

Table 8 also summarises the pore properties of the samples, showing that it was possible to make c-MMC with very different pore sizes in a controlled manner. By adjusting the gel/powder formation rate in the powder-formation

step of the synthesis, the average size of the mesopores in the c-MMC samples could be tuned from ~3 nm to ~20 nm.

In Figure 18, information gathered from the pore-size control study is used to obtain a schematic representation of how the pores are formed in the material. In short, the MMC material was constructed from the aggregated nanoparticles; firstly, **Type I** nanoparticles (with dimensions around 2-5 nm) aggregated to form **Type II** nanoparticles (~30 nm in size), and then the aggregation of **Type II** nanoparticles formed the basis of the MMC material during drying and the solid powder formation process.

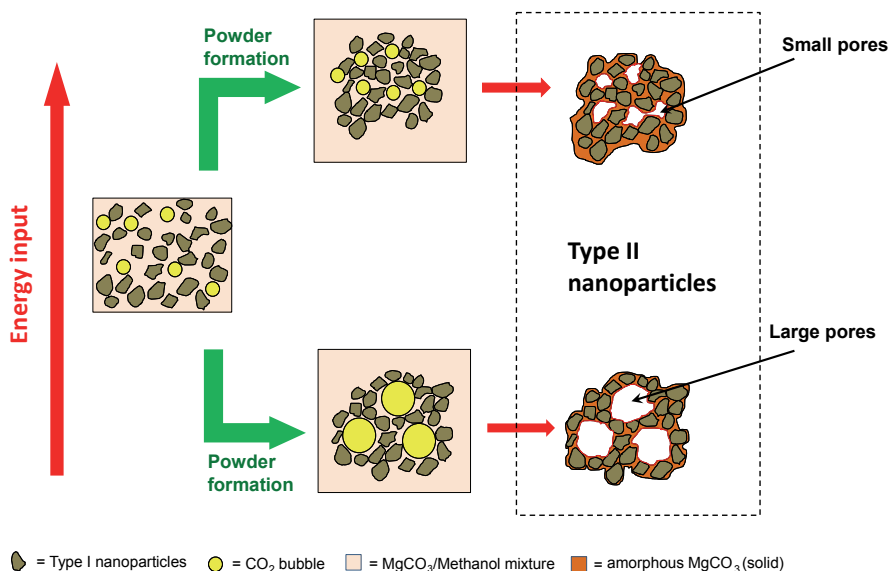


*Figure 18.* Schematic representation of the mechanism and energy input (e.g. temperature or stirring) related to the pore formation in MMC.

Figure 18 also shows how the pore size can be controlled by adjusting the energy input during the powder formation step of the synthesis. Here, the energy input represents any potential energy change to the system, including heating, stirring and so on.

During the powder formation step, a large amount of  $\text{CO}_2$  is given off from the reaction mixture. In the reaction mixture,  $\text{CO}_2$  molecules aggregate to form bubbles to reduce the surface energy. Nanometer-sized particles of MMC (**Type I** and **Type II** nanoparticles) assemble around these  $\text{CO}_2$  bubbles which are then essentially trapped in this configuration. Low temperatures allow the  $\text{CO}_2$  molecules to form aggregates in the reaction mixture to a higher extent than at high temperatures, due to the slower kinetics. The lower temperature (slow kinetics) resulted in larger bubbles and subsequently larger pores. Sample D (Table 8) demonstrated the effect of reduced energy input (by removing stirring, compared with sample C) clearly, since it

had the largest pore size compared to the other samples. After the wet powder forms, the pores can be fixed by heating under N<sub>2</sub> flow. This step fixes the shape of the assembled powder particles and removes the trapped CO<sub>2</sub> bubbles, resulting in a porous solid.

### 5.1.3 Surface Modification of MMC

Surface modification of c-MMC was carried out as described in Section 4.2 (Paper V). Two m-MMCs, with different levels of amine coverage, were obtained. The amine coverage was determined from elemental analysis; the coverage of the two samples was ~1.2 and ~1.7 molecules/nm<sup>2</sup>. We named the samples m-MMC-1.2APTES and m-MMC-1.7APTES in this thesis. After the amine modification, the m-MMC particles were still porous with a high surface area (Table 9); the pore size decreased with increasing amine coverage. All m-MMC samples remained X-ray-certified amorphous (Figure 19) which indicates that the amorphous structure of the materials did not change after the amine modification.

Table 9. Properties of different levels of c-MMC and the two m-MMCs.

|  | c-MMC | m-MMC-1.2APTES | m-MMC-1.7APTES |
|--|-------|----------------|----------------|
| <b>Amine loading (1/nm<sup>2</sup>)</b>  | 0     | 1.17           | 1.68           |
| <b>S<sub>BET</sub> (m<sup>2</sup>/g)</b> | 608   | 601            | 509            |
| <b>Peak DFT pore diameter (nm)</b>       | 5.0   | 4.5            | 4.0            |
| <b>Pore volume (cm<sup>3</sup>/g)</b>    | 0.82  | 0.65           | 0.50           |

IR was also employed to investigate the m-MMC samples. The lower panels in Figure 19 show infrared spectra for c-MMC and m-MMC-1.7APTES; the bands related to the APTES of m-MMC are visible from the infrared spectra. A series of infrared bands related to C-H vibration modes was observed around 2800-3000 cm<sup>-1</sup>. The bands at 2930 and 2885 cm<sup>-1</sup> were assigned to the asymmetric and symmetric stretching modes, respectively, of -CH<sub>2</sub> on the propyl groups from APTES; these bands were similar to those observed on amine-modified mesoporous silica samples [103, 104]. An additional band at 2974 cm<sup>-1</sup> was observed for the amine m-MMC. The two bands at around 3275 and 3340 cm<sup>-1</sup> were assigned to N-H asymmetric stretching and symmetric stretching modes of the amine group, respectively. Infrared bands that were characteristic of magnesium carbonate, such as the carbonate asymmetric stretching band at around 1440 cm<sup>-1</sup> and the carbonate symmetric stretching band at 1076 cm<sup>-1</sup>, were present in both samples.

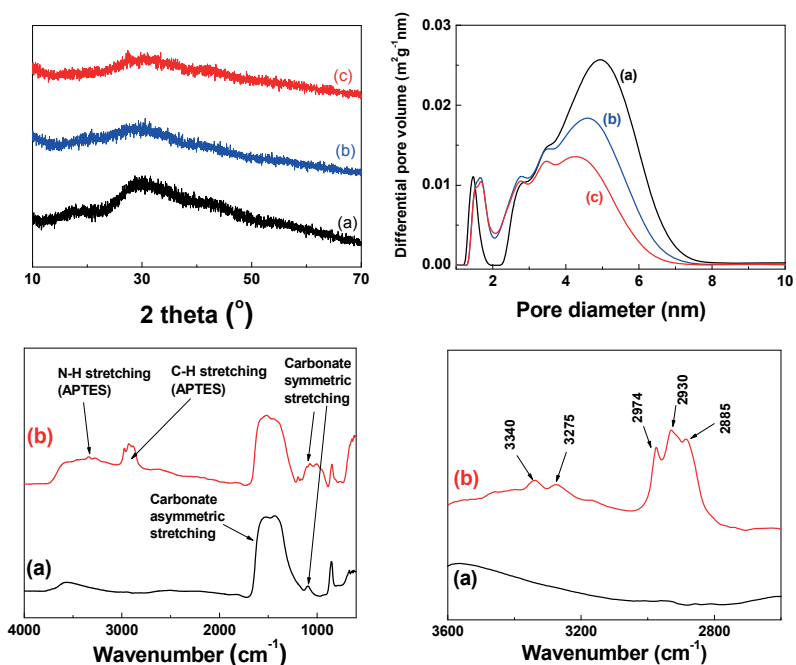


Figure 19. Left top: XRD patterns of c-MMC (black), m-MMC-1.2APTES (blue) and m-MMC-1.7APTES (red); right top: DFT pore-size distribution of c-MMC (black), m-MMC-1.2APTES (blue) and m-MMC-1.7APTES (red); bottom: infrared spectra of c-MMC (black) and m-MMC-1.7APTES (red).

The pore sizes in m-MMC were smaller than those in the unmodified c-MMC (Table 9) as expected, since part of the free space in the pores was most likely occupied by the introduced molecules. Figure 19 also shows a comparison of the DFT pore-size distributions of the samples. It was noted that as the amine coverage increased, the pores reduced in diameter. The modification reduced the overall pore volume as well, because of the addition of the grafted APTES molecules. The larger pores (diameter larger than 4 - 5 nm) appeared to be more susceptible to amine grafting, as demonstrated by the larger decrease in pore volume for these larger pores, as well as the relatively small decrease in the BET surface area (as small pores contribute more to the overall specific surface area).

## 5.2 Physical properties of loaded APIs

### 5.2.1 State of loaded APIs

In this thesis, solvent evaporation method was used to incorporate the APIs into MMC, c-MMC and m-MMC. Papers II and V confirmed that, after the API loading, there was no observed change in the shape of MMC and m-

MMC; they retained the irregular shapes they had before the loading procedure.

To study the physical state of the loaded API, ibuprofen-loaded samples (c-MMC-IBU and m-MMC-IBU) were analysed using XRD and DSC; the results are presented in Figure 20.

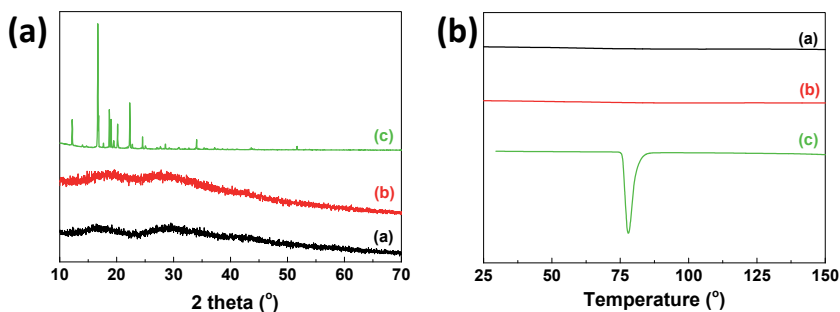


*Figure 20.* (a) XRD patterns of c-MMC-IBU (black), m-MMC-IBU (red) and pure ibuprofen (green); (b) DSC curves for the studied samples: c-MMC-IBU (black), m-MMC-IBU (red) and pure ibuprofen (green). Here, c-MMC loaded with ibuprofen sample was named as c-MMC-IBU, ibuprofen loaded into m-MMC sample was named m-MMC-IBU.

The XRD patterns indicated that neither c-MMC-IBU nor m-MMC-IBU showed a visible peak arising from the crystalline structure of ibuprofen. The lack of peaks in these samples determined that the IBU incorporated in the c-MMC and m-MMC samples was amorphous. This was further confirmed by DSC analysis. The endothermic peak at 78 °C for pure ibuprofen corresponds to the melting process of the crystalline structure (melting point). No peaks corresponding to any endo- or exothermic event were detected in the DSC scan between 25 °C and 150 °C for the c-MMC-IBU and m-MMC-IBU samples, confirming that the incorporated IBU was not present in the crystalline state inside the pores. XRD and DSC data proved that the mesoporous structure of c-MMC and m-MMC completely suppressed the crystallisation of the incorporated APIs, thus stabilising their amorphous state.

### 5.2.2 Characterisation of the porous structure after API loaded

A summary of the pore volume, surface area and pore diameter characterisation results for the c-MMC and m-MMC-1.7APTES samples is given in Table 10. When these values are compared with the information in Table 9, it is clear that the porosity of the m-MMC-1.7APTES and c-MMC samples decreased by half after loading the drug (named as c-MMC-IBU and m-MMC-1.7APTES-IBU, respectively). The reduction in pore volume and the

decrease in pore width is a clear indication that the ibuprofen molecules were incorporated into the pore structure of the MMC samples.

Table 10. Properties of c-MMC and m-MMC samples loaded with ibuprofen<sup>a</sup>.

|  | c-MMC-IBU | m-MMC-1.7APTES-IBU |
|--|-----------|--------------------|
| $S_{\text{BET}}$ ( $\text{m}^2/\text{g}$ ) | 400       | 263                |
| DFT peak pore diameter (nm)                | 4.5       | 3.5                |
| Pore volume ( $\text{cm}^3/\text{g}$ )     | 0.44      | 0.21               |

a) The samples were loaded with ~20 wt.% of ibuprofen (calculated from the TGA analysis).

## 5.3 *In vitro* release study

### 5.3.1 Release mechanism study

The kinetics of the release of the model drug ibuprofen (IBU) from MMC were investigated in Paper I. The dissolution profiles of crystalline IBU and IBU incorporated in MMC are shown in Figure 21.

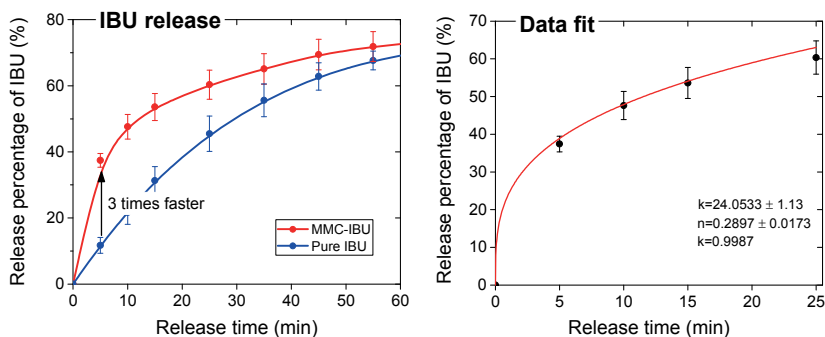


Figure 21. Left panel: Dissolution profiles for crystalline ibuprofen and ibuprofen incorporated in MMC. Right panel: the initial 60% of ibuprofen released from the MMC-IBU sample fitted to the Korsmeyer-Peppas equation  $M_t/M_\infty = kt^n$ . The obtained fitting parameters are displayed. All release measurements were performed in phosphate buffer (pH 6.8) in triplicate. The data are displayed as mean values with corresponding standard deviations.

The release profiles clearly indicate that the incorporated IBU dissolved (i.e. released) more rapidly than the free substance. During the first 5 min, the dissolution rate for the amorphous IBU from the MMC-IBU sample was three times higher than that of the crystalline IBU; 50% of the IBU was released from the MMC and dissolved within 12 min, while it took 30 min for 50% of the crystalline substance to be dissolved.

In order to examine the mechanism of ibuprofen release from the MMC particles, the release data were fitted to the Korsmeyer-Peppas equation:

$$\frac{M_t}{M_\infty} = kt^n$$

where  $M_t$  and  $M_\infty$  are the amounts of drug released at times  $t$  and  $\infty$ , respectively, measured as the concentrations in solution;  $M_t/M_\infty$  is the fraction of the drug released;  $k$  is the kinetic constant;  $t$  is the time and  $n$  is the diffusion exponent, which is used to differentiate the various release mechanisms [105-107]. The Korsmeyer-Peppas equation is valid for the first 60% of the drug that is released and can be used to analyse the mechanism of release from non-swelling matrices (Table 11). For a spherical non-swelling system, Fickian diffusion, anomalous (non-Fickian) transport and zero-order release mechanisms can be discriminated from each other by the diffusion exponent  $n$ ; an  $n$  of 0.43 represents purely Fickian diffusion while an  $n$  of 1.0 indicates zero-order release. A value between 0.43 and 1.0 corresponds to some combination of release mechanisms or to non-Fickian transport.

Table 11. Diffusion exponent and mechanism of diffusional release from various non-swelling controlled-release systems [105].

| Diffusion exponent, $n$ |                    |                  | Drug-release mechanism            |
|-------------------------|--------------------|------------------|-----------------------------------|
| Thin film               | Cylindrical sample | Spherical sample |                                   |
| 0.50                    | 0.45               | 0.43             | Fickian diffusion                 |
| $0.50 < n < 1.0$        | $0.45 < n < 1.0$   | $0.43 < n < 1.0$ | Anomalous (non-Fickian) transport |
| 1.0                     | 1.0                | 1.0              | Zero-order release                |

The  $n$ -value for the MMC-IBU samples was calculated as  $\sim 0.29$  from the parameters shown in Figure 21, indicating a release mechanism that is exclusively diffusion-limited from MMC particles with a wide size distribution [105].

### 5.3.2 Regulated release from MMC

This section discusses the methods used to regulate the speed of release from MMC; the experimental details are given in the published papers.



### 5.3.2.1 Release from different particle sizes of MMC

The release of APIs from well defined particle-size fractions of MMC was studied to further investigate the potential of MMC as a drug-delivery vehicle and to tune the release profile. The dissolution profiles of the model drug ibuprofen from the different MMC-IBU samples are displayed in Figure 22.

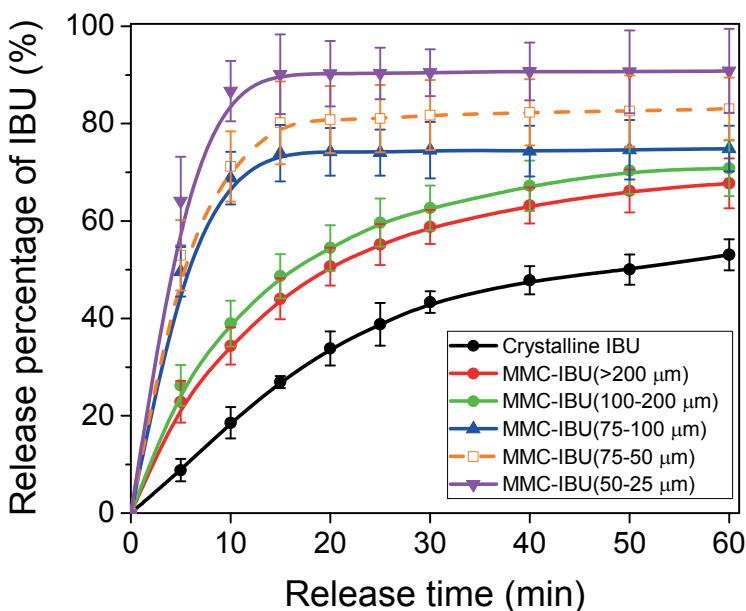
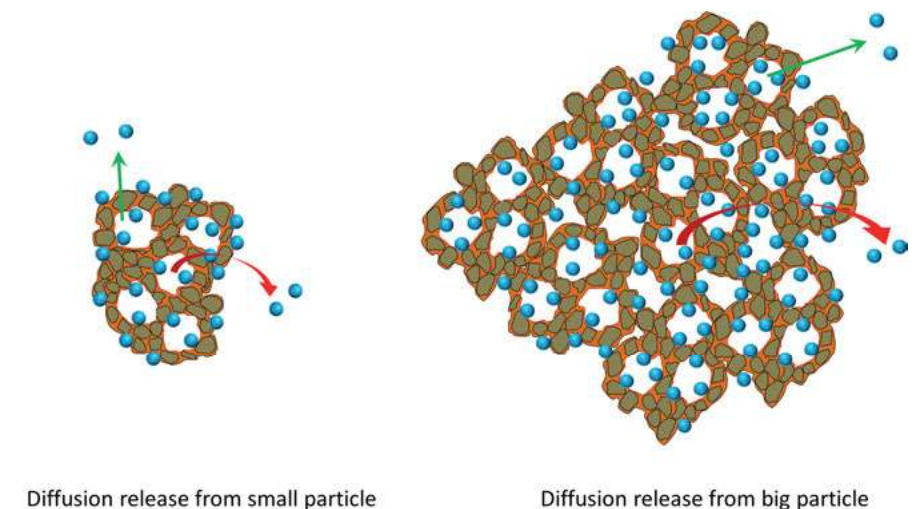


Figure 22. Release profiles of ibuprofen from MMC of different particle sizes. The values on the y-axis are given as percentages of the total amounts of ibuprofen present in dissolved form in the dissolution vessel (phosphate buffer, pH 6.8). For all release curves, 100% corresponds to an ibuprofen concentration of 40 mg/L.

The dissolution profile indicates that the initial dissolution rate of crystalline ibuprofen was considerably slower than the dissolution rate of the loaded drug after release from the MMC-IBU samples of varying particle size.

After the first 5 min, only approximately 8% of ibuprofen was dissolved in the buffer from the crystalline ibuprofen sample; however, this percentage tended to increase for the loaded drug when the MMC particle size decreased, reaching over 60% for the smallest particle size fraction investigated (between 50 and 25  $\mu\text{m}$ ). This concentration was not even reached after 60 min of exposure to the dissolution medium for the crystalline drug. As seen from the dissolution profile, the rate reached a plateau after about 15 min for MMC-IBU (50 - 25  $\mu\text{m}$ ) but not for MMC-IBU (> 200  $\mu\text{m}$ ) which continued releasing ibuprofen past 60 min. This is likely due to that the diffusion dis-

tance for ibuprofen through the material was longer for the larger particles (Figure 23).



*Figure 23.* Illustration of the possible diffusion release mechanism from different particle sizes of MMC-IBU. While the diffusion distance will highly influence the diffusion rate, it takes longer for the substance to diffuse over a longer distance, thus lowering the diffusion rate.

### 5.3.2.2 Release from MMC with different pore sizes

In Paper III, the drug itraconazole (ITZ) was loaded into c-MMC samples with three different average pore sizes (~5.1 nm, ~13 nm and ~20 nm). The loaded itraconazole was confirmed as being in an amorphous state by DSC and XRD analysis, as in the ibuprofen release study. Nitrogen adsorption results of loaded and unloaded samples are shown in Table 12.

Table 12. Specific surface area and pore properties of different c-MMC-ITZ samples<sup>a,b</sup>.

|  | c-MMC5 | c-MMC13 | c-MMC20 | c-MMC5-ITZ | c-MMC13-ITZ | c-MMC20-ITZ |
|--|--------|---------|---------|------------|-------------|-------------|
| $S_{\text{BET}}(\text{m}^2/\text{g})$                  | 618    | 263     | 173     | 434        | 186         | 141         |
| <b>DFT peak pore diameter (nm)</b>                     | ~5.1   | ~13     | ~20     | ~4.4       | ~11.3       | ~15         |
| <b>Pore volume (<math>\text{cm}^3/\text{g}</math>)</b> | 0.76   | 1.27    | 1.00    | 0.50       | 0.74        | 0.59        |

a) c-MMC5, c-MMC13 and c-MMC20 represent c-MMC samples with DFT pore-size distributions of ~5.1 nm, ~13 nm and ~20 nm, respectively.

b) The loading percentage for all samples was 30 wt.%, as calculated by TGA.

The time-resolved release of itraconazole from the ground carrier particles (particle size  $\leq 100 \mu\text{m}$ ) into simulated gastric fluid (pH  $\sim 1.3$ ) is shown in Figure 24. As shown in the figure, the release rate from c-MMC20-ITZ during the first 30 min was enhanced by a factor of  $\sim 23$  compared to the dissolution rate of crystalline itraconazole. The corresponding release rate enhancements for c-MMC13-ITZ and c-MMC5-ITZ were  $\sim 17$  and  $\sim 13$ , respectively.

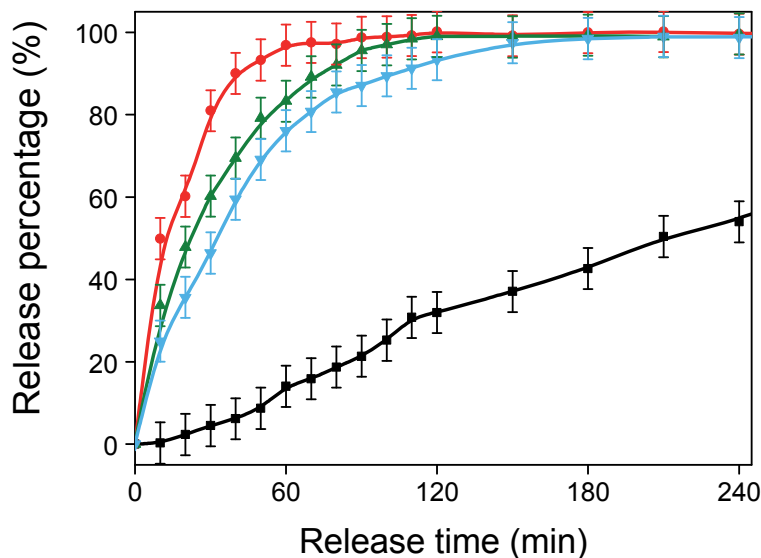


*Figure 24.* Time-resolved release in simulated gastric fluid (pH 1.3) of itraconazole from c-MMCs powder with average pore sizes of 20 nm (red curve), 13 nm (green curve) and 5.1 nm (blue curve) as well as dissolution rate of the crystalline drug (black curve). Before the release test, the c-MMC-ITZ samples were ground to small particles (particle size  $\leq 100 \mu\text{m}$ , decided by SEM).

It was noted that c-MMC could dissolve under such acidic conditions; however, during the first 30 min, there were no visible changes to the powder in the dissolution vessel (pH 1.3). The time required for the full release of itraconazole differed between c-MMC drug carriers with different pore sizes (see Table 13). The carrier with the largest pore size (c-MMC20-ITZ) fully released the drug molecules in the shortest time (about 60 min). This was noticeably faster than the c-MMC with smaller pore sizes and the crystalline form of the drug, as anticipated.

Table 13. Release profile of itraconazole from c-MMC-ITZ samples with different pore sizes.

| Sample                                   | c-MMC20-ITZ | c-MMC13-ITZ | c-MMC5-ITZ | Pure ITZ |
|--|-------------|-------------|------------|----------|
| Percentage released after 10 minutes (%) | 50          | 35          | 25         | 0.15     |
| 50% release time (min)                   | 10          | 22          | 35         | 240      |
| 100% release time (min)                  | 60          | 90          | 180        | --       |

### 5.3.2.3 Release from modified MMC

In order to investigate whether the change in the rate of release of ibuprofen from MMC was related to the presence of the amine groups, MMC was also modified using N-propyltriethoxysilane (PTES), which has a similar chemical structure to APTES but does not have an amine group. The release profiles are shown in Figure 25; the left panel shows the release profiles for the two samples of modified MMC with different levels of amine coverage, and the right panel shows the release profiles for m-MMC-APTES and m-MMC-PTES.

The initial ibuprofen release rate decreased significantly with increasing amine density on the surface of the m-MMC (Figure 25 left). After 30 min, over 95% of the loaded ibuprofen had been released from the unmodified sample (c-MMC-IBU), while 85% and 68% of the loaded drug was released from the amine-modified samples, m-MMC-1.2APTES-IBU and m-MMC-1.7APTES-IBU, respectively, within the same time period. The m-MMC-APTES samples continued to release IBU under the tested conditions after this time. Between 30 and 180 min after the start of the experiment, m-MMC-1.2APTES-IBU had released an additional 5% of the loaded ibuprofen and m-MMC-1.7APTES-IBU had released an additional 10%. As m-MMC-1.8PTES-IBU and m-MMC-1.7APTES-IBU samples had a similar grafting density (1.76 PTES/nm<sup>2</sup>, 1.68 APTES/nm<sup>2</sup>, respectively), the release of ibuprofen from these two samples was compared, to investigate the effects of amine functionalisation. Figure 25 also clearly shows that the PTES-modified sample released ibuprofen more rapidly than the APTES-modified sample from the beginning.

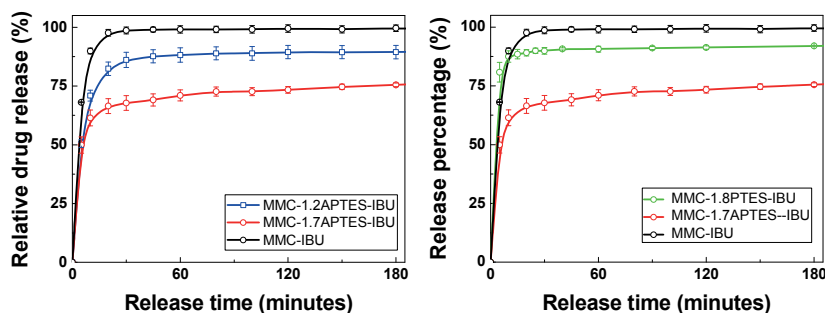


*Figure 25.* Release profiles of ibuprofen from modified and unmodified MMC samples. The values on the y-axis are the amounts of ibuprofen dissolved in the phosphate buffer (pH 6.8) in the dissolution vessel as a percentage of the total amount added (40 mg/L). In all samples, the ibuprofen loading percentage was ~ 20 wt.% (calculated by TGA).

The introduction of amine groups on the surface of MMC had a significant effect on the release of loaded ibuprofen that can be explained by the increased interaction between the matrix and the ibuprofen molecules. This is believed to be caused by hydrogen-bonding interactions between the carboxyl groups of ibuprofen and the amine groups of the modified material. The increase in amine modification thus enhanced the interaction (a stronger hydrogen-bonding interaction) between the carrier  $\text{-NH}_2$  groups on the surface with the  $\text{-OH}$  groups of the drug; however, as there is no corresponding functional group in the PTES molecule that can form a strong interaction with ibuprofen, the release of ibuprofen from the PTES-modified sample was significantly faster than from the APTES-modified sample. Figure 26 provides an illustration of how the chemistry of the surface of the modified MMC is hypothesized to affect the release rate of the loaded ibuprofen.

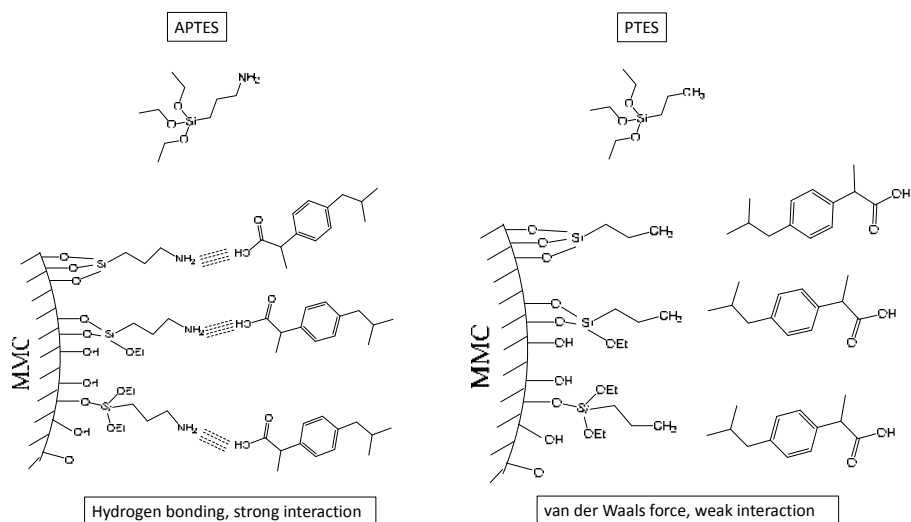


Figure 26. Representation of the potential interaction between the surface groups on m-MMC and the loaded ibuprofen molecule.

## 5.4 *In vitro* drug release of APIs reaching supersaturation

In Paper IV, the general applicability of MMC as drug delivery system was investigated. Three BCS II drugs - celecoxib (CEL), cinnarizine (CIN) and griseofulvin (GRI) - with different proteolytic functions were used to investigate the possibility that the increase in release rate from MMC could trigger supersaturation of poorly soluble APIs and consequently improve their bioavailability. All three drugs were successfully loaded in their non-crystalline form into MMC and rapidly released from this carrier (Figure 27).

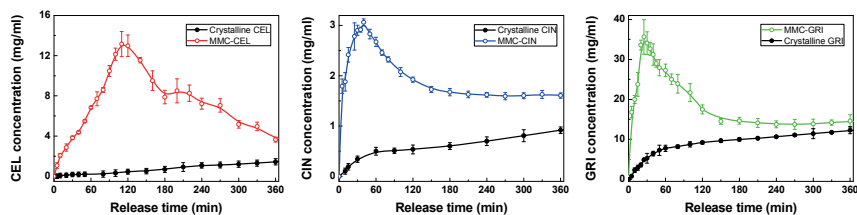


Figure 27. Release profiles showing the concentration of celecoxib, cinnarizine and griseofulvin over time, after release from MMC samples, compared with the crystalline API. The y-axis shows the concentration of the API in phosphate buffer (pH 6.8, 37 °C) in the dissolution vessel.

A summary of the pharmacokinetic parameters ( $AUC_{0-240}$ ,  $C_{MAX}$  and  $T_{MAX}$ ) calculated from the dissolution profiles of the crystalline drugs, showing that the release of the drugs from MMC resulted in supersaturation, is presented

in Table 14. The results show a significant increase in  $C_{MAX}$  and AUC and a decrease in  $T_{MAX}$  for all three drugs when released from MMC as compared to the crystalline drug. For celecoxib,  $C_{MAX}$  was 11.3  $\mu\text{g/mL}$ , which was 2.9 times higher than for the crystalline form, and the  $AUC_{0-240}$  was 25 times higher for MMC-CEL than for crystalline celecoxib. The concentration after supersaturation slowly declined until it returned to a level corresponding to the crystalline solubility after approximately 360 minutes. Similar results were observed for the release of cinnarizine and griseofulvin after supersaturation: the  $AUC_{0-240}$  of cinnarizine from MMC-CIN was 5.4 times higher than that of crystalline CIN while, for MMC-GRI, this value was 2.2 times higher.

From these results, it is evident that loading the APIs into MMC can enhance both the rate and the extent of released APIs. Hence, MMC appears to be a valuable new addition to the toolbox of drug-delivery vehicles that may be used to achieve a more rapid onset of therapeutic effect and/or to extend the absorption phase after oral delivery.

Table 14. Summary of calculated pharmacokinetic parameters for celecoxib, cinnarizine and griseofulvin between 0 and 240 min.

|  | Pure drug | Supersaturation Release |
|--|-----------|-------------------------|
| <b>Celecoxib</b>                             |           |                         |
| $C_{MAX}(\mu\text{g/ml})$                    | 1.1       | 11.3                    |
| $T_{MAX}(\text{min})$                        | 240       | 112                     |
| $AUC_{0-240}(\mu\text{g}\cdot\text{min/ml})$ | 70        | 1692                    |
| <b>Cinnarizine</b>                           |           |                         |
| $C_{MAX}(\mu\text{g/ml})$                    | 0.7       | 2.1                     |
| $T_{MAX}(\text{min})$                        | 240       | 40                      |
| $AUC_{0-240}(\mu\text{g}\cdot\text{min/ml})$ | 62        | 340                     |
| <b>Griseofulvin</b>                          |           |                         |
| $C_{MAX}(\mu\text{g/ml})$                    | 10.5      | 34.8                    |
| $T_{MAX}(\text{min})$                        | 240       | 25                      |
| $AUC_{0-240}(\mu\text{g}\cdot\text{min/ml})$ | 2063      | 4567                    |

$C_{MAX}$ , maximum concentration;  $T_{MAX}$ , time to reach maximum concentration; AUC, area under the concentration-time curve.

## 6. Summary and Conclusions

MMC was evaluated as a drug carrier that offers enhanced stability of the amorphous (more water-soluble) form and subsequent solubility enhancement of otherwise poorly water-soluble APIs. In the release control study, the strategies investigated indicated that the release of the loaded APIs was tunable by altering the particle size, the pore size and the surface functionalisation of the MMC. This study is the basis for further development of MMC as a drug carrier.

It was ascertained after loading into MMC that the APIs remained in the amorphous state, and it was found that this amorphous state was stabilised by the mesoporous structure of MMC. When ibuprofen, which is a well studied, poorly soluble BCS II API, was incorporated in its amorphous form into MMC, it was found that its solubility was significantly improved compared to the crystalline form. The release of ibuprofen from MMC occurred by diffusion.

Several strategies for controlling the release of the loaded APIs from MMC were investigated; these included tuning the particle size and the pore size and altering the surface modifications. Comparison of the release of the API from samples with different particle sizes and pore sizes resulted in a better understanding of the effects of tailoring the release of APIs from MMC. It was found that bigger particle sizes and/or smaller pore sizes resulted in slower release rates.

Further work showed that the surface properties of MMC can be tuned by changing the type of organic chemical used. The choice of functional groups on the molecules was the key in controlling the drug-release rate. Specifically, amine groups were found to have enhanced interaction with the drug molecule, reducing the initial release rate.

The presented work shows that MMC has great potential for use as a DDS for poorly soluble APIs under development. The API-loaded MMC samples resulted in supersaturated solutions of the APIs, potentially increasing their bioavailability.



## 7. Future work

MMC, which is still a relatively new material in the mesoporous materials field, has been confirmed in this thesis for potential use as a drug carrier that can help to improve the solubility of poorly aqueous-soluble APIs. However, there are still many other possible applications to be investigated. For example, modified MMC could be tailored in a different way to be used for the absorption and separation of chemicals.

In this work, only *in vitro* dissolution tests were performed. *In vivo* human pharmacokinetic studies, which are the “standard” for assessing the bioequivalence of APIs, are required. The oral toxicity of MMC should be investigated *in vivo* and the biocompatibility of the different MMC materials with different surface-functionalised groups should also be studied.

## 8. Svensk sammanfattning

En stor andel av de läkemedelskandidater som framställs inom dagens läkemedelsutveckling är svårösliga i vatten och har därför ingen eller begränsad terapeutisk effekt om de administreras oralt i sin rena form. Anledningen är att läkemedel behöver kunna lösas upp i vätskan inuti mag-tarmkanalen för att ha möjlighet att passera genom tarmväggen. Den låga lösligheten hos läkemedelskandidater utgör därför en stor utmaning inom läkemedelsutveckling där orala beredningar i form av kapslar och tableter ofta är önskvärdt. För många läkemedel är alternativet till oral administration intravenösa injektioner vilket är både kostsamt för sjukvården och hindrar patienter från att sköta sin egen medicinering eftersom den måste utföras av behörig personal vid vårdinrättningar.

Ett antal olika formuleringsstrategier har därför tagits fram för att kringgå detta problem. Att bilda salter av läkemedelssubstanser och att minska partikelstorleken på läkemedelskristaller är två vanliga exempel på detta. Alla strategier har sina respektive för- och nackdelar men eftersom substanser har olika fysiokemiska egenskaper så finns det inte en universallösning som är lämpad att öka lösligheten hos alla svårösliga substanser.

På senare tid har man uppmärksammat möjligheten att utnyttja att substanser som befinner sig i sin amorfa fas, det vill säga en oordnad icke-kristallin fas, har en högre skenbar löslighet jämfört med samma substans som befinner sig i en kristallin fas. Anledningen är att det amorfa tillståndet innebär ett termodynamiskt högre energitillstånd hos substansen vilket gör att bindingarna mellan läkemedelsmolekylerna är lättare att bryta än om samma substans har kristalliserat. Att formulera läkemedelssubstanser i sin amorfa fas framstår därför som ett attraktivt alternativ för att lösa problematiken med låg löslighet hos läkemedelssubstanser. På grund av det termodynamiskt höga energitillståndet har amorfa substanser dock en benägenhet att spontant kristalliseras om de inte stabiliseras på något vis. I det avseendet är mesoporösa material intressanta att använda som hjälpämnen i läkemedelsformuleringar eftersom de kan hindra kristallisation av substanser som inkorporeras i materialet. Mesoporösa material är material som innehåller porer i storleksordningen 2-50 nm. Porerne i materialet hindrar läkemedelsmolekyler från att bilda kristaller på grund av det begränsade utrymmet samt den höga ytenergin i de nanometerstora porerna. Mesoporösa material har förmåga att hindra kristallisation av läkemedelssubstanser samt bevara dessa i sina amorfa faser under lång tid.

Huvudmålet med denna avhandling var att undersöka möjligheten att använda mesoporös magnesiumkarbonat som läkemedelsbärare för att öka lösligheten samt upplösningshastigheten av läkemedel med låg vattenlöslighet. En rad olika modellsubstanser med olika fysiokemiska egenskaper användes i arbetet där den mesoporösa magnesiumkarbonaten visade sig ha möjlighet att effektivt hindra kristallisation av alla dessa modellsubstanser. Detta resulterade i både högre löslighet och ökad frisättningshastighet av substanserna vilket i en klinisk situation skulle kunna översättas till både ökad terapeutisk effekt och snabbare verkan. Detta är någonting som kommer att undersökas längre fram i samband med det fortsatta arbetet i projektet.

Dessutom visades att frisättningshastigheten kunde styras genom att justera materialet partikelstorlek och porstorlek. Slutligen visades att ytan på materialet kan funktionaliseras med amingrupper vilket bidrog till att frisättningshastigheten på ibuprofen kunde förlängas tack vare interaktioner mellan amingrupperna och ibuprofen.

Sammantaget visar arbetet att mesoporös magnesiumkarbonat kan fungera som ett hjälpämne i läkemedelsformuleringar både för att öka löslighet hos svårslösliga substanser samt för att styra frisättningshastighet av dessa. Tack vare den enkla syntesen av den mesoporösa magnesiumkarbonaten, där de enda råvarorna som behövs är magnesiumoxid, metanol och koldioxid, framstår detta material som ett spännande hjälpämne för att formulera svårslösliga läkemedelskandidater och möjliggöra att de kan kommersialiseras och komma till klinisk användning.

## 9. Acknowledgements

When I was writing this page, I realized that my 4 years PhD study was almost finished. It's really unbelievable how time flies.

First and foremost, I would like to express my deepest gratitude to my supervisor *Maria Strømme*, thank you for providing me with the opportunity to study in the nanotechnology and functional materials group under your guidance. You are a fantastic person who knows how to encourage people and whenever I had obstacles, you were always there and helped me overcome. Your enthusiasm to science, invaluable guidance and supports help me to grow as a scientist.

I would also like to thank my co-supervisor *Johan Gómez de la Torre*, thank you for helping and teaching me a lot, no matter in the lab or in the life. You are genius at photography, the SEM images and poster illustrations, they are super beautiful.

*Teresa Zardán Gómez de la Torre*, thank you for your patient guidance and help. Every time I came to you for help, you always tried your best to help me. You are so optimistic, even if you have to travel from Stockholm to Uppsala every day.

My co-supervisor *Christel Bergström* at the department of pharmacy at BMC, thank you for teaching me a lot in drug delivery and pharmacokinetics knowledge. I know when I have questions about pharmaceutical technologies, you are the person that I can ask.

My co-supervisor *Ken Welch*, thank you for your kind help with many things, you are our great support.

*Albert Mihrianyan*, thank you for discussing and sharing your knowledge with me. And you look like Kong Fu master when you wear that Chinese style shirt.

*Ocean Cheung*, I am so glad that I met you in this group. I really appreciate for your sharing your knowledge about porous materials and also ASAP. Thanks to your crazy enthusiasm, we did thousands of isotherms in 3 months. I would also especially to thank you for proofreading this thesis. And also thank you for answering my call at anytime, even after 24:00 in the morning.

*Sara Frykstrand Ångström*, thank you for everything you've done for me. You are the wonderful friend. From my start, you taught me a lot about this project and instruments. Thank you for so many inspirational discussions! I really enjoy the collaborations with you.

*Kai Hua*, 师兄, wish you are here to celebrate this moment. You are the first Chinese I met in Uppsala, I still remembered that you pick me up at Uppsala Centralstation the first day I arrived.

Thank you all my co-authors, *Natalia Ferraz, Zhaohui Wang, Petter Tammela, Daniel O. Carlsson, Haoquan Zheng, Taimin Yang, Marco Sommariva, Xiaodong Zou* for invaluable research contributions.

Thanks for all my projects colleagues, *Maria Vall, Rui Sun, Ao Gao, Philip Erenbo, Changqing Ruan and Jiaojiao Yang*, you are fantastic people to work with.

I would say thank you to all my group mates, *Li, Martin, Jonas, Yanling, Henrik, Christoffer, Rikard, Joakim, Simon, Hao, Mia, Gopi, Lisa, Alex, Jun, Changgang and Igor*, it is great pleasure to work with you these years.

For assistance with administration, computers, and chemicals, I would like to thank *Ingrid Ringård, Per-Richard Lindgren, Jonatan Bagge, Maria Melin and Maria Skoglund*.

I would also like to express my gratitude to *Yanling Cai & Di Wu, Xiaohu Guo, Wen Huang, Da Zhang & Man Song, Song Chen & Shu Li, Hu Li & Jiangwei Liu, Jinbao Zhang, Yi Ren & Xiaowen Li, Mingzhi Jiao & Yurong Hu, Bing Cai, Wei Xia, Cong Su, Lingshuang Kong, Tao Qing, Dou Du, Xi Chen, Ming Gao, Yiming Zou & Lina Qu, Lei Tian, Jun Luo, Yue Ma, Le Fu, Ruijun Pan & Qiuhong Wang, Yixiao Cai, Liang Dai & Zhen Cao, Jia Liu, Hanqian Zhang & Xue Zhao, Ping Yan, Fei Huang & Na Xiu, Yu Zhang, Lei Zhang, Liyang Shi & Jingyi Hong, Yuanyuan Han, Chao Xu, Xiao Huang, Jinxing Huo, Yifan Wang, Yizhang Huang, Xinxin Huang & Johan, Huayi Lin*. You guys have made me feel at home in Uppsala.

最后我要感谢我的家人。感谢我的姥爷，姥姥和奶奶，谢谢你们对我的爱；感谢我的爸爸妈妈，谢谢你们一直以来的关怀；感谢我的岳父岳母，谢谢你们培养如此优秀的女儿。

最后，我要特别感谢我的妻子，谢谢你来到我的生命中，为我带来美好。你是我生命的支撑，在瑞典的四年，你放弃了你在国内的一切来陪伴我，让我可以全身心地读博的道路上拼搏；纵然会有坎坷挫折，可有你在背后一如既往的支持，让我坚持了下来。有你，真好。

青螺添远山。两娇靥，笑时圆。

抱云勾雪近灯看。

**妍**处不堪怜。

今生但愿无离别，花月下，绣屏前。

双蚕成茧共缠绵。更结后生缘。

-- 张先 《庆金枝》

# References

- [1] L.X. Yu, E. Lipka, J.R. Crison, G.L. Amidon, Transport approaches to the biopharmaceutical design of oral drug delivery systems: Prediction of intestinal absorption, *Adv Drug Deliv Rev*, 19 (1996) 359-376.
- [2] R. Lobenberg, G.L. Amidon, Modern bioavailability, bioequivalence and biopharmaceutics classification system. New scientific approaches to international regulatory standards, *Eur J Pharm Biopharm*, 50 (2000) 3-12.
- [3] G.L. Amidon, H. Lennernas, V.P. Shah, J.R. Crison, A Theoretical Basis for a Biopharmaceutic Drug Classification - the Correlation of in-Vitro Drug Product Dissolution and in-Vivo Bioavailability, *Pharmaceutical Research*, 12 (1995) 413-420.
- [4] E. Merisko-Liversidge, G.G. Liversidge, E.R. Cooper, Nanosizing: a formulation approach for poorly-water-soluble compounds, *Eur J Pharm Sci*, 18 (2003) 113-120.
- [5] C. Leuner, J. Dressman, Improving drug solubility for oral delivery using solid dispersions, *Eur J Pharm Biopharm*, 50 (2000) 47-60.
- [6] T. Vasconcelos, B. Sarmiento, P. Costa, Solid dispersions as strategy to improve oral bioavailability of poor water soluble drugs, *Drug Discov Today*, 12 (2007) 1068-1075.
- [7] N. Nasongkla, A.F. Wiedmann, A. Bruening, M. Beman, D. Ray, W.G. Bornmann, D.A. Boothman, J.M. Gao, Enhancement of solubility and bioavailability of beta-lapachone using cyclodextrin inclusion complexes, *Pharmaceut Res*, 20 (2003) 1626-1633.
- [8] N.J. Babu, A. Nangia, Solubility Advantage of Amorphous Drugs and Pharmaceutical Cocrystals, *Cryst Growth Des*, 11 (2011) 2662-2679.
- [9] J.C. DiNunzio, D.A. Miller, W. Yang, J.W. McGinity, R.O. Williams, Amorphous Compositions Using Concentration Enhancing Polymers for Improved Bioavailability of Itraconazole, *Mol Pharm*, 5 (2008) 968-980.
- [10] M. Vallet-Regi, A. Ramila, R.P. del Real, J. Perez-Pariante, A new property of MCM-41: Drug delivery system, *Chem Mater*, 13 (2001) 308-311.
- [11] M. Vallet-Regi, F. Balas, D. Arcos, Mesoporous materials for drug delivery, *Angew Chem Int Edit*, 46 (2007) 7548-7558.
- [12] M.E. Davis, Ordered porous materials for emerging applications, *Nature*, 417 (2002) 813-821.
- [13] A. Vu, Y.Q. Qian, A. Stein, Porous Electrode Materials for Lithium-Ion Batteries - How to Prepare Them and What Makes Them Special, *Adv Energy Mater*, 2 (2012) 1056-1085.
- [14] Y. Yu, C.H. Chen, Y. Shi, A Tin-Based Amorphous Oxide Composite with a Porous, Spherical, Multideck-Cage Morphology as a Highly Reversible Anode Material for Lithium-Ion Batteries, *Adv Mater*, 21 (2009) 3541-3541.

- [15] S.E. Kim, J.H. Park, Y.W. Cho, H. Chung, S.Y. Jeong, E.B. Lee, I.C. Kwon, Porous chitosan scaffold containing microspheres loaded with transforming growth factor-beta1: implications for cartilage tissue engineering, *J Control Release*, 91 (2003) 365-374.
- [16] M. Vallet-Regi, I. Izquierdo-Barba, M. Colilla, Structure and functionalization of mesoporous bioceramics for bone tissue regeneration and local drug delivery, *Philos Trans A Math Phys Eng Sci*, 370 (2012) 1400-1421.
- [17] C. Vincent, Process for producing low-bulk density silica, U.S. Patent Publication, 1971.
- [18] C.T. Kresge, M.E. Leonowicz, W.J. Roth, J.C. Vartuli, J.S. Beck, Ordered Mesoporous Molecular-Sieves Synthesized by a Liquid-Crystal Template Mechanism, *Nature*, 359 (1992) 710-712.
- [19] C. Barbe, J. Bartlett, L.G. Kong, K. Finnie, H.Q. Lin, M. Larkin, S. Calleja, A. Bush, G. Calleja, Silica particles: A novel drug-delivery system, *Adv Mater*, 16 (2004) 1959-1966.
- [20] J.C. Doadrio, E.M.B. Sousa, I. Izquierdo-Barba, A.L. Doadrio, J. Perez-Pariente, M. Vallet-Regi, Functionalization of mesoporous materials with long alkyl chains as a strategy for controlling drug delivery pattern, *J Mater Chem*, 16 (2006) 462-466.
- [21] S. Simovic, N. Ghouchi-Eskandar, A.M. Sinn, D. Losic, C.A. Prestidge, Silica materials in drug delivery applications, *Curr Drug Discov Technol*, 8 (2011) 250-268.
- [22] S. Kwon, R.K. Singh, R.A. Perez, E.A. Abou Neel, H.W. Kim, W. Chrzanowski, Silica-based mesoporous nanoparticles for controlled drug delivery, *J Tissue Eng*, 4 (2013) 1-35.
- [23] J.S. Beck, J.C. Vartuli, W.J. Roth, M.E. Leonowicz, C.T. Kresge, K.D. Schmitt, C.T.W. Chu, D.H. Olson, E.W. Sheppard, S.B. Mccullen, J.B. Higgins, J.L. Schlenker, A New Family of Mesoporous Molecular-Sieves Prepared with Liquid-Crystal Templates, *J Am Chem Soc*, 114 (1992) 10834-10843.
- [24] A. Monnier, F. Schuth, Q. Huo, D. Kumar, D. Margolese, R.S. Maxwell, G.D. Stucky, M. Krishnamurty, P. Petroff, A. Firouzi, M. Janicke, B.F. Chmelka, Cooperative Formation of Inorganic-Organic Interfaces in the Synthesis of Silicate Mesostructures, *Science*, 261 (1993) 1299-1303.
- [25] F. Ciuchi, G. Dinicola, H. Franz, G. Gottarelli, P. Mariani, M.G.P. Bossi, G.P. Spada, Self-Recognition and Self-Assembly of Folic-Acid Salts - Columnar Liquid-Crystalline Polymorphism and the Column Growth-Process, *J Am Chem Soc*, 116 (1994) 7064-7071.
- [26] S. Che, A.E. Garcia-Bennett, T. Yokoi, K. Sakamoto, H. Kunieda, O. Terasaki, T. Tatsumi, A novel anionic surfactant templating route for synthesizing mesoporous silica with unique structure, *Nat Mater*, 2 (2003) 801-805.
- [27] P. van Hoogevest, X.L. Liu, A. Fahr, Drug delivery strategies for poorly water-soluble drugs: the industrial perspective, *Expert Opin Drug Del*, 8 (2011) 1481-1500.
- [28] A. Fahr, X. Liu, Drug delivery strategies for poorly water-soluble drugs, *Expert Opin Drug Del*, 4 (2007) 403-416.
- [29] M.N. Martinez, G.L. Amidon, A mechanistic approach to understanding the factors affecting drug absorption: A review of fundamentals, *J Clin Pharmacol*, 42 (2002) 620-643.
- [30] U.S. Food and Drug Administration, Waiver of In Vivo Bioavailability and Bioequivalence Studies for Immediate-Release Solid Oral Dosage Forms Based on a Biopharmaceutics Classification System, (2000).

- [31] U.S. Food and Drug Administration, Guidance for Industry: Bioavailability and Bioequivalence Studies for Oral Administered Drug Products—General Considerations, (2003).
- [32] S. Stegemann, F. Leveiller, D. Franchi and H. Lindén, When poor solubility becomes an issue: from early stage to proof of concept, *Eur J Pharm Sci*, 31(2007) 249-261.
- [33] L. Dittert, W. Cressman, S. Kaplan, S. Riegelman, J. Wagner, Guidelines for biopharmaceutical studies in man, American Pharmaceutical Association, Academy of Pharmaceutical Sciences, (1972).
- [34] V. Di Tullio, M. Cocca, R. Avolio, G. Gentile, N. Proietti, P. Ragni, M.E. Errico, D. Capitani, M. Avella, Unilateral NMR investigation of multifunctional treatments on stones based on colloidal inorganic and organic nanoparticles, *Magn Reson Chem*, 53 (2015) 64-77.
- [35] C.A. Lipinski, F. Lombardo, B.W. Dominy, P.J. Feeney, Experimental and computational approaches to estimate solubility and permeability in drug discovery and development settings, *Adv Drug Deliv Rev*, 23 (1997) 3-25.
- [36] C.A. Lipinski, Drug-like properties and the causes of poor solubility and poor permeability, *J Pharmacol Toxicol*, 44 (2000) 235-249.
- [37] E. Nelson, Solution Rate of Theophylline Salts and Effects from Oral Administration, *J Am Pharm Assoc*, 46 (1957) 607-614.
- [38] E. Nelson, Comparative Dissolution Rates of Weak Acids and Their Sodium Salts, *J Am Pharm Assoc*, 47 (1958) 297-299.
- [39] S.H. Yalkowsky, J.F. Krzyzaniak, G.H. Ward, Formulation-related problems associated with intravenous drug delivery, *J Pharm Sci*, 87 (1998) 787-796.
- [40] S. Gaisford, M. Saunders, Essentials of pharmaceutical preformulation, (2012).
- [41] J. Rautio, H. Kumpulainen, T. Heimbach, R. Oliyai, D. Oh, T. Jarvinen, J. Savolainen, Prodrugs: design and clinical applications, *Nat Rev Drug Discov*, 7 (2008) 255-270.
- [42] K.M. Huttunen, H. Raunio, J. Rautio, Prodrugs—from Serendipity to Rational Design, *Pharmacol Rev*, 63 (2011) 750-771.
- [43] D.H. Jornada, G.F.D. Fernandes, D.E. Chiba, T.R.F. de Melo, J.L. dos Santos, M.C. Chung, The Prodrug Approach: A Successful Tool for Improving Drug Solubility, *Molecules*, 21 (2016).
- [44] N. Blagden, M. de Matas, P.T. Gavan, P. York, Crystal engineering of active pharmaceutical ingredients to improve solubility and dissolution rates, *Adv Drug Deliv Rev*, 59 (2007) 617-630.
- [45] M. Vogt, K. Kunath, J.B. Dressman, Dissolution enhancement of fenofibrate by micronization, cogrinding and spray-drying: Comparison with commercial preparations, *Eur J Pharm Biopharm*, 68 (2008) 283-288.
- [46] E.M. Merisko-Liversidge, G.G. Liversidge, Drug Nanoparticles: Formulating Poorly Water-Soluble Compounds, *Toxicol Pathol*, 36 (2008) 43-48.
- [47] N. Rasenack, B.W. Muller, Dissolution rate enhancement by in situ micronization of poorly water-soluble drugs, *Pharmaceutes Res*, 19 (2002) 1894-1900.
- [48] M. Sugimoto, T. Okagaki, S. Narisawa, Y. Koida, K. Nakajima, Improvement of dissolution characteristics and bioavailability of poorly water-soluble drugs by novel cogrinding method using water-soluble polymer, *Int J Pharmaceut*, 160 (1998) 11-19.
- [49] P.J. Marsac, T. Li, L.S. Taylor, Estimation of drug-polymer miscibility and solubility in amorphous solid dispersions using experimentally determined interaction parameters, *Pharm Res*, 26 (2009) 139-151.



- [50] F. Qian, J. Huang, M.A. Hussain, Drug-Polymer Solubility and Miscibility: Stability Consideration and Practical Challenges in Amorphous Solid Dispersion Development, *J Pharm Sci*, 99 (2010) 2941-2947.
- [51] A. Forster, J. Hempenstall, T. Rades, Characterization of glass solutions of poorly water-soluble drugs produced by melt extrusion with hydrophilic amorphous polymers, *J Pharm Pharmacol*, 53 (2001) 303-315.
- [52] A.L. Sarode, P. Wang, S. Obara, D.R. Worthen, Supersaturation, nucleation, and crystal growth during single- and biphasic dissolution of amorphous solid dispersions: Polymer effects and implications for oral bioavailability enhancement of poorly water soluble drugs, *Eur J Pharm Biopharm*, 86 (2014) 351-360.
- [53] E. Karavas, G. Ktistis, A. Xenakis, E. Georganakis, Effect of hydrogen bonding interactions on the release mechanism of felodipine from nanodispersions with polyvinylpyrrolidone, *Eur J Pharm Biopharm*, 63 (2006) 103-114.
- [54] S. Janssens, G. Van den Mooter, Review: physical chemistry of solid dispersions, *Journal of Pharmacy and Pharmacology*, 61 (2009) 1571-1586.
- [55] M.E. Aulton, K.M. Taylor, *Aulton's pharmaceuticals: the design and manufacture of medicines*, Elsevier Health Sciences, (2013).
- [56] C. Bhugra, M.J. Pikal, Role of thermodynamic, molecular, and kinetic factors in crystallization from the amorphous state, *J Pharm Sci*, 97 (2008) 1329-1349.
- [57] W.H. Lim, M.J. Lawrence, Influence of surfactant and lipid chain length on the solubilisation of phosphatidylcholine vesicles by micelles comprised of polyoxyethylene sorbitan monoesters, *Colloid Surf A*, 250 (2004) 449-457.
- [58] C.W. Pouton, Formulation of poorly water-soluble drugs for oral administration: Physicochemical and physiological issues and the lipid formulation classification system, *Eur J Pharm Sci*, 29 (2006) 278-287.
- [59] M.S. Bakshi, How Surfactants Control Crystal Growth of Nanomaterials, *Cryst Growth Des*, 16 (2016) 1104-1133.
- [60] J. Rouquerol, D. Avnir, C.W. Fairbridge, D.H. Everett, J.H. Haynes, N. Pernicone, J.D.F. Ramsay, K.S.W. Sing, K.K. Unger, Recommendations for the Characterization of Porous Solids, *Pure Appl Chem*, 66 (1994) 1739-1758.
- [61] E. Robens, F. Rouquerol, J. Rouquerol, K. Sing, *Adsorption by powders and porous solids*, Academic Press, London, UK, 1999.
- [62] K.E. Hendrickson III, *The encyclopedia of the industrial revolution in world history*, (2014).
- [63] X.S. Zhao, G.Q.M. Lu, G.J. Millar, Advances in mesoporous molecular sieve MCM-41, *Ind Eng Chem Res*, 35 (1996) 2075-2090.
- [64] B. Munoz, A. Ramila, J. Perez-Pariente, I. Diaz, M. Vallet-Regi, MCM-41 organic modification as drug delivery rate regulator, *Chem Mater*, 15 (2003) 500-503.
- [65] P. Horcajada, A. Ramila, J. Perez-Pariente, M. Vallet-Regi, Influence of pore size of MCM-41 matrices on drug delivery rate, *Micropor Mesopor Mat*, 68 (2004) 105-109.
- [66] A.L. Doadrio, E.M.B. Sousa, J.C. Doadrio, J.P. Pariente, I. Izquierdo-Barba, M. Vallet-Regi, Mesoporous SBA-15 HPLC evaluation for controlled gentamicin drug delivery, *J Control Release*, 97 (2004) 125-132.
- [67] X. Xia, K. Pethe, R. Kim, L. Ballell, D. Barros, J. Cechetto, H. Jeon, K. Kim, A.E. Garcia-Bennett, Encapsulation of Anti-Tuberculosis Drugs within Mesoporous Silica and Intracellular Antibacterial Activities, *Nanomaterials*, 4 (2014) 813-826.

- [68] R. Mellaerts, J.A.G. Jammaer, M. Van Speybroeck, H. Chen, J. Van Humbeeck, P. Augustijns, G. Van den Mooter, J.A. Martens, Physical state of poorly water soluble therapeutic molecules loaded into SBA-15 ordered mesoporous silica carriers: A case study with itraconazole and ibuprofen, *Langmuir*, 24 (2008) 8651-8659.
- [69] E. Makila, M.P.A. Ferreira, H. Kivela, S.M. Niemi, A. Correia, M.A. Shahbazi, J. Kauppila, J. Hirvonen, H.A. Santos, J. Salonen, Confinement Effects on Drugs in Thermally Hydrocarbonized Porous Silicon, *Langmuir*, 30 (2014) 2196-2205.
- [70] S.C. Shen, W.K. Ng, L. Chia, J. Hu, R.B.H. Tan, Physical state and dissolution of ibuprofen formulated by co-spray drying with mesoporous silica: Effect of pore and particle size, *Int J Pharm*, 410 (2011) 188-195.
- [71] S.C. Shen, W.K. Ng, L. Chia, Y.C. Dong, R.B.H. Tan, Stabilized Amorphous State of Ibuprofen by Co-Spray Drying With Mesoporous SBA-15 to Enhance Dissolution Properties, *J Pharm Sci*, 99 (2010) 1997-2007.
- [72] J. Alie, J. Menegotto, P. Cardon, H. Duplaa, A. Caron, C. Lacabanne, M. Bauer, Dielectric study of the molecular mobility and the isothermal crystallization kinetics of an amorphous pharmaceutical drug substance, *J Pharm Sci*, 93 (2004) 218-233.
- [73] Y. Aso, S. Yoshioka, S. Kojima, Molecular mobility-based estimation of the crystallization rates of amorphous nifedipine and phenobarbital in poly(vinylpyrrolidone) solid dispersions, *J Pharm Sci*, 93 (2004) 384-391.
- [74] A.R. Bras, E.G. Merino, P.D. Neves, I.M. Fonseca, M. Dionisio, A. Schonhals, N.T. Correia, Amorphous Ibuprofen Confined in Nanostructured Silica Materials: A Dynamical Approach, *J Phys Chem C*, 115 (2011) 4616-4623.
- [75] S. Mann, S.L. Burkett, S.A. Davis, C.E. Fowler, N.H. Mendelson, S.D. Sims, D. Walsh, N.T. Whilton, Sol-gel synthesis of organized matter, *Chem Mater*, 9 (1997) 2300-2310.
- [76] J.Y. Ying, C.P. Mehnert, M.S. Wong, Synthesis and applications of supramolecular-templated mesoporous materials, *Angew Chem Int Edit*, 38 (1999) 56-77.
- [77] X. Feng, G.E. Fryxell, L.Q. Wang, A.Y. Kim, J. Liu, K.M. Kemner, Functionalized monolayers on ordered mesoporous supports, *Science*, 276 (1997) 923-926.
- [78] S.W. Song, K. Hidajat, S. Kawi, Functionalized SBA-15 materials as carriers for controlled drug delivery: Influence of surface properties on matrix-drug interactions, *Langmuir*, 21 (2005) 9568-9575.
- [79] B.G. Trewyn, I.I. Slowing, S. Giri, H.T. Chen, V.S.Y. Lin, Synthesis and functionalization of a mesoporous silica nanoparticle based on the sol-gel process and applications in controlled release, *Accounts Chem Res*, 40 (2007) 846-853.
- [80] C. Göltner-Spickermann, Non-ionic templating of silica: formation mechanism and structure, *Curr Opin Colloid Interface Sci*, 7 (2002) 173-178.
- [81] A. Sayari, S. Hamoudi, Periodic mesoporous silica-based organic - Inorganic nanocomposite materials, *Chem Mater*, 13 (2001) 3151-3168.
- [82] H.J. Kim, H.C. Yang, D.Y. Chung, I.H. Yang, Y.J. Choi, J.K. Moon, Functionalized Mesoporous Silica Membranes for CO<sub>2</sub> Separation Applications, *J Chem*, (2015).
- [83] Y. Belmabkhout, A. Sayari, Effect of pore expansion and amine functionalization of mesoporous silica on CO<sub>2</sub> adsorption over a wide range of conditions, *Adsorption*, 15 (2009) 318-328.

- [84] J. Aguado, J.M. Arsuaga, A. Arencibia, M. Lindo, V. Gascon, Aqueous heavy metals removal by adsorption on amine-functionalized mesoporous silica, *J Hazard Mater*, 163 (2009) 213-221.
- [85] L. Mercier, T.J. Pinnavaia, Access in mesoporous materials: Advantages of a uniform pore structure in the design of a heavy metal ion adsorbent for environmental remediation, *Adv Mater*, 9 (1997) 500-503.
- [86] W.M. Van Rhijn, D.E. De Vos, B.F. Sels, W.D. Bossaert, P.A. Jacobs, Sulfonic acid functionalised ordered mesoporous materials as catalysts for condensation and esterification reactions, *Chem Commun*, (1998) 317-318.
- [87] J. Forsgren, S. Frykstrand, K. Grandfield, A. Mihranyan, M. Strømme, A Template-Free, Ultra-Adsorbing, High Surface Area Carbonate Nanostructure, *Plos One*, 8 (2013).
- [88] R.C. Rowe, P.J. Sheskey, P.J. Weller, *Handbook of pharmaceutical excipients*, Pharmaceutical press London 2006.
- [89] U.S. Food and Drug Administration, Food additive status list, US Food and Drug Administration (FDA), Rockville, (2006).
- [90] R.F. Haines-Nutt, The compression properties of magnesium and calcium carbonates, *J Pharm Pharmacol*, 28 (1976) 468-470.
- [91] T.M. Cham, The Effect of the Specific Surface-Area of Heavy Magnesium Carbonate on Its Tableting Properties, *Drug Dev Ind Pharm*, 13 (1987) 1989-2015.
- [92] N.A. Armstrong, T.M. Cham, Changes in the Particle-Size and Size Distribution during Compaction of 2 Pharmaceutical Powders with Dissimilar Consolidation Mechanisms, *Drug Dev Ind Pharm*, 12 (1986) 2043-2059.
- [93] M. Sandor, A. Riechel, I. Kaplan, E. Mathiowitz, Effect of lecithin and  $MgCO_3$  as additives on the enzymatic activity of carbonic anhydrase encapsulated in poly(lactide-co-glycolide) (PLGA) microspheres, *Biochim Biophys Acta*, 1570 (2002) 63-74.
- [94] S.O. Aideloje, C.O. Onyeji, N.C. Ugwu, Altered pharmacokinetics of halofantrine by an antacid, magnesium carbonate, *Eur J Pharm Biopharm*, 46 (1998) 299-303.
- [95] F. Lu, S.H. Wu, Y. Hung, C.Y. Mou, Size Effect on Cell Uptake in Well-Suspended, Uniform Mesoporous Silica Nanoparticles, *Small*, 5 (2009) 1408-1413.
- [96] R. Ryoo, S.H. Joo, M. Kruk, M. Jaroniec, Ordered mesoporous carbons, *Adv Mater*, 13 (2001) 677-681.
- [97] R.I. Nooney, D. Thirunavukkarasu, Y.M. Chen, R. Josephs, A.E. Ostafin, Synthesis of nanoscale mesoporous silica spheres with controlled particle size, *Chem Mater*, 14 (2002) 4721-4728.
- [98] C.E. Fowler, D. Khushalani, B. Lebeau, S. Mann, Nanoscale materials with mesostructured interiors, *Adv Mater*, 13 (2001) 649-652.
- [99] S. Frykstrand, J. Forsgren, A. Mihranyan and M. Strømme, On the pore forming mechanism of Upsalite, a micro- and mesoporous magnesium carbonate, *Micropor. Mesopor. Mat.* 190 (2014) 99-104.
- [100] D.H. Lee, M. Choi, B.W. Yu, R. Ryoo, Organic functionalization of mesopore walls in hierarchically porous zeolites, *Chem Commun*, (2009) 74-76.
- [101] A. Datt, I. El-Maazawi, S.C. Larsen, Aspirin Loading and Release from MCM-41 Functionalized with Aminopropyl Groups via Co-condensation or Postsynthesis Modification Methods, *J Phys Chem C*, 116 (2012) 18358-18366.

- [102] E. Ahmadi, N. Dehghannejad, S. Hashemikia, M. Ghasemnejad, H. Tabebordbar, Synthesis and surface modification of mesoporous silica nanoparticles and its application as carriers for sustained drug delivery, *Drug Deliv*, 21 (2014) 164-172.
- [103] Z. Bacsik, R. Atluri, A.E. Garcia-Bennett, N. Hedin, Temperature-Induced Uptake of CO<sub>2</sub> and Formation of Carbamates in Mesocaged Silica Modified with n-Propylamines, *Langmuir*, 26 (2010) 10013-10024.
- [104] Z. Bacsik, N. Ahlsten, A. Ziadi, G.Y. Zhao, A.E. Garcia-Bennett, B. Martin-Matute, N. Hedin, Mechanisms and Kinetics for Sorption of CO<sub>2</sub> on Bicontinuous Mesoporous Silica Modified with n-Propylamine, *Langmuir*, 27 (2011) 11118-11128.
- [105] P.L. Ritger, N.A. Peppas, A simple equation for description of solute release I. Fickian and non-Fickian release from non-swellable devices in the form of slabs, spheres, cylinders or discs, *J Control Release*, 5 (1987) 23-36.
- [106] P.L. Ritger, N.A. Peppas, A simple equation for description of solute release II. Fickian and anomalous release from swellable devices, *J Control Release*, 5 (1987) 37-42.
- [107] N.A. Peppas, J.J. Sahlin, A simple equation for the description of solute release. III. Coupling of diffusion and relaxation, *Int J Pharmaceut*, 57 (1989) 169-172.



# Acta Universitatis Upsaliensis

*Digital Comprehensive Summaries of Uppsala Dissertations  
from the Faculty of Science and Technology 1433*

Editor: The Dean of the Faculty of Science and Technology

A doctoral dissertation from the Faculty of Science and Technology, Uppsala University, is usually a summary of a number of papers. A few copies of the complete dissertation are kept at major Swedish research libraries, while the summary alone is distributed internationally through the series Digital Comprehensive Summaries of Uppsala Dissertations from the Faculty of Science and Technology. (Prior to January, 2005, the series was published under the title “Comprehensive Summaries of Uppsala Dissertations from the Faculty of Science and Technology”.)

Distribution: [publications.uu.se](http://publications.uu.se)  
urn:nbn:se:uu:diva-303832



ACTA  
UNIVERSITATIS  
UPSALIENSIS  
UPPSALA  
2016